Effects of manufacturing direction, heat-treatment and surface operations on fatigue life in additively manufactured metals: An analysis based on statistics and artificial intelligence.

YAREN, Mehmet F <http://orcid.org/0000-0002-7739-0794>, JOHN, Edward <http://orcid.org/0000-0002-8707-4197> and SUSMEL, Luca <http://orcid.org/0000-0001-7753-9176>

Citation:

Copyright and re-use policy

Effects of manufacturing direction, heat-treatment and surface operations on fatigue life in additively manufactured metals: An analysis based on statistics and artificial intelligence

Mehmet F Yaren[1,2] iD, Edward John[2] iD and Luca Susmel[3] iD

Abstract

This study aimed to establish whether useful fatigue design stress-life curves could be estimated for additively manufactured metals through statistical and machine learning analysis of a large quantity of experimental fatigue data. The study focused on additively manufactured aluminium, steel and titanium. Three manufacturing parameters were considered, namely the manufacturing direction, heat-treatment and surface operations, with the results presented for 0.1 and −1 loading ratios. By gathering experimental data for all parameters, the negative inverse slopes were found to be concentrated between 3 and 6, and the mean endurance limit as a ratio to ultimate tensile strength was 0.18 and 0.21 for 0.1 and −1 loading ratios, respectively, without any statistical analysis. Surface operations were observed to have a significant effect on the fatigue strength of additively manufactured aluminium, steel and titanium regardless of other manufacturing parameters. Multiple linear regression analysis and several machine learning methods (Decision Tree, Support Vector Machines, K-Nearest Neighbour, Multi-Layer Perceptron, Partial Least Squares and Gaussian Process Regression) were used to develop predictive models. The results of these analyses highlight that the conventional approach applied to fatigue of traditional metals does not suffice for additively manufactured metals. While artificial intelligence presents a promising solution, our investigation indicates it is necessary to account for parameters in addition to those considered here such as manufacturing processes, material properties, material microstructure and defects to make reliable fatigue property estimates for additively manufactured metals using machine learning.

Introduction

Additive manufacturing (AM) has significant potential to develop production processes, offering advantages in many industries. Additive manufacturing makes it possible to design the interior part of products and produce complex geometries easily. This technology has simplified the design and production of many components in sectors such as aviation, energy, healthcare, automotive and defence. For example, it has been used to create lightweight components like brackets and to produce complex parts for engines in the aviation industry.[1] In healthcare, additive manufacturing enables personalised health solutions, such as customised implants, prosthetics and stents, thereby increasing the success rate of treatments. It is also widely used in energy applications for turbines and heat exchangers. Furthermore, additive manufacturing is a popular choice for design and research teams due to its rapid and cost-effective prototyping capabilities.

[1]Department of Mechanical Engineering, Sakarya University, Sakarya, Türkiye
[2]School of Mechanical, Aerospace and Civil Engineering, Sir Frederick Mappin Building, The University of Sheffield, Sheffield, UK
[3]Materials and Engineering Research Institute, Sheffield Hallam University, Sheffield, UK

Corresponding author:
Luca Susmel, Materials and Engineering Research Institute, Sheffield Hallam University, Harmer Building, Sheffield S1 1WB, UK.
Email: l.susmel@shu.ac.uk

Techniques in additive manufacturing are developing, and this technology is becoming more affordable. Although additive manufacturing reduces material waste and its efficiency is high, the full benefit of this efficiency is not yet seen in the end product cost, mainly due to the cost of materials. New printing approaches, production technologies, parameters and materials are continually being developed and researched. Moreover, the characteristics of additively manufactured parts, as well as the effects of parameters on these characteristics, are topics of scientific research, and experimental data is increasing in the literature rapidly.

The production parameters of additive manufactured components can significantly affect the resultant mechanical properties and fatigue performance. Understanding the impact of manufacturing parameters on the material's fatigue strength is crucial for industrial applications. However, there are no standard rules that engineers can follow to construct approximate SN curves when designing additively manufactured components against high-cycle fatigue loading. The following literature review summarises some recent work done in the field of characterising the high-cycle fatigue performance of additively manufactured materials.

Materials including polymers, metals, concrete and ceramics, are used in additive manufacturing. Among these materials, metal-based materials have garnered significant interest for industrial application. Additive manufacturing methods used in producing metal parts can be categorised into two main groups: Power Bed Fusion (PBF) and Directed Energy Deposition (DED). PBF further divides into laser (L-PBF) or electron beam (E-PBF) based approaches. In DED method, the material can be in the form of either powder or wire. Additionally, there are some rarely used different methods in the literature like bound metal deposition, binder jetting etc. Each method includes different production parameters such as power, current, voltage, material feed rate, etc.

There are a limited number of studies in the literature that compare the effects of different production methods.[2–20] The studies generally investigate the effects of chemical compounds of metals,[21–23] manufacturing orientation,[6,24–33] heat treatment,[4,34–45] and surface operations.[29,39,46–54] In some studies about additively manufactured metals, researchers investigated the effects of materials and production methods on fatigue behaviour.

Sun et al.[28] investigated the effect of manufacturing orientation on Ti-6Al-4V specimens produced using Selective Laser Melting (SLM). A significant influence of manufacturing orientation on the fatigue performance of this alloy is reported. Chang et al.[32] and Qian et al.[30] also found that fatigue performance changed with different manufacturing orientations on the mentioned material with SLM but with annealed conditions. On the other hand, Persenot et al.[27] used a machined specimen made of Ti-6Al-4V via EBM, and they could not observe any significant difference in fatigue properties related to manufacturing orientation. SLM is also used in two other studies by Yadollahi et al.[26] and Zhao et al.[25] to produce specimens made of 17-4 PH and AlSi12Mg alloys, respectively. Both studies highlight the significant influence of build direction on fatigue. Yadollahi et al.[26] explain the difference in fatigue strength between specimens with different manufacturing orientations by considering the alignment of deposited layers relative to the loading axis. Zhao et al.[25] found that horizontally built specimens exhibited a higher fatigue life than vertically built ones for a similar pore size. On the other hand, Nezhadfar et al.[24] tested AIF357, ALSi10Mg and AD1 specimens produced with the L-PBF method but did not observe any differences in fatigue strength related to build orientation. In summary, the literature is divided regarding influence of build direction relative to loading direction on the fatigue strength of additively manufactured titanium or aluminium specimens.

Nezhadfar et al.[47] found that performing a solution heat treatment before other heat treatment procedures, such as ageing, significantly improved the fatigue strength of their as-built 17-4 PH specimens produced with the L-PBF method. Baek et al.[55] discuss AlSi10Mg material produced by SLM, finding that direct ageing of the alloy gave the best fatigue properties, while the T6 alloy had the lowest fatigue limit. Another study by Schneller et al.[45] using AlSi10Mg produced through SLM shows that the effect of heat treatment depends on the process temperature. For example, heat treatments below a specific temperature can worsen fatigue properties of AlSi10Mg. Hot isostatic pressing is revealed to be more effective than heat treatments for improving the fatigue life of Ti-6Al-4V produced through L-PBF.[56] Kaletsch et al.[36] and Ardi et al.[44] both focused on Inconel 718 material produced by L-PBF. High fatigue strengths were achieved after hot isostatic pressing, even with high initial porosity and argon content. However, there may be a critical limit for high porosity when specimens after hot isostatic pressing are subjected to heat treatment without pressure.[36] According to a study by Ardi et al.,[44] hot isostatic pressing is found to be effective in reducing porosities and decreasing the porosity volume ratio. However, it may not always contribute to enhancing the fatigue performance of Inconel 718 parts. This may be due to the presence of inclusions and brittle phases within the material, as well as a reduction in yield strength caused by hot isostatic pressing. The literature therefore shows that heat treatment processes can have a positive influence on the fatigue strength of additively manufactured titanium, steel and aluminium specimens, however, a positive effect is not guaranteed and the process must be carefully selected for each material.

The effect of machining on fatigue life has also been investigated in the literature. Ti-6Al-4V produced by EBM showed lower fatigue resistance in as-built specimens than machined ones.[27] Lee et al.[57] indicated that laser polishing and stress relief significantly improved fatigue strength in Ti-6Al-4V produced via L-PBF. Witkin et al.[29] found that surface condition played a more important role in fatigue strength than the specimen orientation for Inconel 718 produced via L-PBF. In another study with the same production method,[58] shot peening improved the fatigue performance of Inconel 625 and Inconel 718. In reference,[47] as expected, better fatigue strength was obtained when the surface of the specimen was machined after heat tempering specimens than for as-built specimens made from 17-4 PH. Therefore, in general, surface operations are reported to improve the fatigue performance of additively manufactured titanium and steel.

From the literature review above, previous studies have explored various factors, including material, manufacturing orientation, post-production treatments and surface conditions. The studies show that the fatigue strength of additively manufactured metals is strongly influenced by complex interactions between the manufacturing and post-processing parameters used. Based on the available literature it is not possible to propose standard rules for estimating design SN curves for additively manufactured metals.

This study aimed to establish whether useful design SN curves could be estimated for additively manufactured metals through statistical and machine learning analysis of a large quantity of experimental fatigue data. The fatigue data used for this analysis was sourced from a recently published database[59] compiling the fatigue and fatigue crack growth behaviours of additively manufactured metals from around 3000 papers. Fatigue data from this database was categorised and re-analysed to determine the SN-curve parameters for each data set. The effectiveness of a multiple linear regression model and several Artificial Intelligence (AI) tools at predicting these SN-curve parameters was then assessed.

Database and the method of the statistical re-analysis

Data filtering and categorisation

In this study, the experimental results are obtained from a database created by Zhang and Xu.[59] The database (FatigueData-AM2022) is generated with the help of machine learning and image processing techniques by using around 3000 scientific papers on fatigue or crack propagation of additively manufactured metals published until the end of 2022. Details of the data, collecting methods and the precision of the data can be seen in reference.[59] The database tabulated the 3D printing parameters, heat treatment processing, fatigue and static test conditions. Some of the data are stress (σ & N) or strain-based (ε & N) fatigue life data, and the others are crack growth rate (da/dN).

This study focused on stress-based fatigue analysis, so, fatigue data sets were only included in the statistical re-analysis if it included stress-life relation data (σ & N) and ultimate stress data under axial tensile loading without any notch effect. Since a small number of data were available for build orientations between 0° and 90°, only the data for build orientations of 0° and 90° were used. The materials given in the database were categorised as either steel (S), aluminium (A) or titanium (T). Post-processing operations were categorised as heat treatment processes and surface operations. Some of the data in the database were heat-treated or hot isostatic pressed, however, for this analysis data was categorised as either heat treated (HT) or not heat treated (NHT). The surface operation categories machining, polishing and both machining and polishing were used to investigate the effect of surface operations on endurance limit in this study. The testing temperature for all data sets analysed was 25° in an air environment, and the tests were load controlled. The feedstock in the data analysed was mostly powder, with only 12 data sets with a wire feedstock. For this reason, feedstock was not considered in the analysis. Only datasets with a Tσ scattering ratio of 2 or less were included in the analysis, for both $P_s = 90\%$ and $P_s = 95\%$. For the statistical assessment and the application of artificial algorithms, z-scores were calculated based on the ratio of σ_{50}/σ_{UTS} and the negative inverse slope values. Data points yielding z-scores greater than 3 were excluded from the statistical evaluations. A summary of the used data is given in Tables 1 and 2.

Fatigue data statistical re-analysis

The fatigue data selected according to the criteria above were statistically re-analysed to obtain fatigue curves for different probabilities of survival ($P_s = 10\%$, 50% and 90%) with the value of endurance limit calculated at 2.10^6 cycles to failure. Fatigue curves can be calculated easily as a straight line in the log-log scale with equation (1), where the endurance limit σ_A corresponds to a number of cycles to failure equal to N_A. N_A is the reference number of cycles to failure, and k is the negative inverse slope. The distribution of fatigue life at a given stress level can be described with a log-normal distribution.[140]

$$\sigma^k . N_f = \sigma_A^k . N_A \qquad (1)$$

Calibration constants are required to obtain a probability of survival by using the least squares linear regression method with the logarithm of life and stress values, as seen in equation (2). The calibration constants, c_0 and c_1 in equation (2) are calculated with

Table 1. Summary of the re-analysed data for 0.1 loading ratio.

Ref.	N. of Data	Angle (°)	Material	Types of AM	Heat treatment	Surface operation	σ_{UTS} (MPa)	k_{50}	σ_{50} (MPa)	σ_{90} (MPa)	$T_{\sigma\,90}$
Kedziora et al.[60]	10	90	17-4 PH	M. Ext.	-	B	496	5.65	64.0	51.1	1.57
Barr et al.[61]	26	0	300M steel	P-DED	-	M	1722	4.96	246.1	197.2	1.56
Barr et al.[61]	4	0	300M steel	P-DED	-	M	1560	13.12	339.5	317.1	1.15
Stern et al.[21]	6	0	316L	L-PBF	NHT	M; P	656	7.35	127.9	118.3	1.17
Zhang et al.[62]	8	0	316L	L-PBF	NHT	Edm; G	723	5.34	147.5	134.3	1.21
Zhang et al.[62]	5	90	316L	L-PBF	NHT	Edm; G	620	7.10	168.4	157.9	1.14
Zhang et al.[63]	7	0	316L	L-PBF	NHT	M	723	4.39	133.2	117.6	1.28
Zhang et al.[63]	6	0	316L	L-PBF	NHT	M	708	5.56	152.3	128.8	1.40
Zhang et al.[63]	9	0	316L	L-PBF	NHT	M	631	6.17	109.8	96.9	1.28
Zhang et al.[63]	9	0	316L	L-PBF	NHT	M	692	5.56	127.0	105.0	1.46
Zhang et al.[63]	4	0	316L	L-PBF	HT	M	673	5.96	139.3	127.1	1.20
Afkhami et al.[64]	13	0	316L	L-PBF	-	M	654	12.39	208.9	198.3	1.11
Afkhami et al.[64]	12	90	316L	L-PBF	-	M	569	11.29	181.0	174.2	1.08
Afkhami et al.[64]	9	90	316L	L-PBF	-	B	553	4.38	110.4	88.4	1.56
Afkhami et al.[64]	5	90	316L	L-PBF	-		647	7.35	170.6	154.7	1.22
Spierings et al.[65]	11	90	316L	L-PBF	-	M	760	4.56	123.0	96.6	1.62
Solberg et al.[66]	13	90	316L	L-PBF	-	B	437	6.15	73.1	65.3	1.25
Thawon et al.[67]	7	0	316L	BMD	HT	B	482	5.92	79.1	72.5	1.19
Voloskov et al.[68]	5	90	316L	L-PBF	NHT	M	565	3.95	126.0	97.7	1.66
Kedziora et al.[60]	8	90	316L	L-PBF	HT	B	533	8.58	139.1	136.9	1.03
Kedziora et al.[60]	8	90	316L	M. Ext.	-	B	314	8.67	51.9	41.1	1.59
Kedziora et al.[60]	9	90	316L	L-PBF	HT	B	571	4.00	94.3	86.8	1.18
Stern et al.[21]	6	0	316L + N	L-PBF	NHT	M; P	714	4.19	113.9	103.3	1.22
He et al.[69]	8	0	Al-5024	L-PBF	NHT	B	304	4.43	33.4	28.5	1.37
He et al.[69]	6	0	Al-5024	L-PBF	HT	B	425	4.15	32.9	26.9	1.49
Lasagni et al.[70]	10	90	Al-Mg-Sc	L-PBF	HT	M	546	7.07	68.2	51.9	1.73
Qin et al.[71]	18	0	Al-Mg-Sc-Zr	L-PBF	HT	M; P	536	5.67	65.1	49.7	1.72
Qin et al.[71]	16	90	Al-Mg-Sc-Zr	L-PBF	HT	M; P	530	4.62	37.1	29.5	1.58
Qin et al.[72]	16	90	Al-Mg-Sc-Zr	L-PBF	HT	M; P	535	4.60	37.2	29.6	1.58
Wu et al.[73]	14	0	AlSi10Mg	L-PBF	HT	G; P	273	5.32	47.9	39.0	1.51
Wu et al.[73]	14	90	AlSi10Mg	L-PBF	HT	G; P	273	4.32	27.6	23.1	1.42
Qian et al.[74]	13	90	AlSi10Mg	L-PBF	HT	M; P	273	4.33	27.6	23.0	1.44
Peng et al.[75]	13	90	AlSi10Mg	L-PBF	-	M; P	273	4.34	27.7	23.0	1.44
Peng et al.[75]	15	0	AlSi10Mg	L-PBF	-	M; P	273	5.35	48.4	39.5	1.50
Yan et al.[76]	8	90	AlSi10Mg	L-PBF	-	P	430	6.18	47.7	41.2	1.34
Beretta et al.[77]	15	90	AlSi10Mg	L-PBF	-	B	469	3.81	26.1	23.2	1.26
Beretta et al.[77]	14	90	AlSi10Mg	L-PBF	-	M	469	6.51	59.7	53.0	1.27
Zhang et al.[78]	15	90	AlSi10Mg	L-PBF	-	V	412	4.41	36.8	31.4	1.38
Zhang et al.[78]	13	90	AlSi10Mg	L-PBF	-	S	412	11.41	65.5	58.4	1.26
Zhang et al.[78]	13	90	AlSi10Mg	L-PBF	-	M; P	412	9.94	76.1	70.4	1.17
Zhao et al.[25]	9	90	AlSi12Mg	L-PBF	-	M	434	6.48	58.0	50.7	1.31
Rao et al.[79]	9	90	AlSi7Mg0.6	L-PBF	HT	B	314	3.35	28.4	23.6	1.45
Rao et al.[79]	5	90	AlSi7Mg0.6	L-PBF	HT	M	327	5.12	62.0	50.6	1.50
Cacace et al.[80]	6	90	AlSi7Mg0.6	L-PBF	HT	S	254	9.78	58.2	54.1	1.15
Cacace et al.[80]	7	90	AlSi7Mg0.6	L-PBF	HT	S	254	8.84	54.5	45.9	1.41
Cacace et al.[80]	11	0	AlSi7Mg0.6	L-PBF	HT	S	254	8.64	51.1	44.4	1.32
Cacace et al.[80]	9	0	AlSi7Mg0.6	L-PBF	HT	S	254	9.51	50.8	46.1	1.22
Wang et al.[81]	4	0	ASTM A131 EH36	L-PBF	-	M; P	971	5.19	149.7	118.4	1.60
Wang et al.[81]	4	0	ASTM A131 EH36	L-PBF	-	M; P	921	5.46	129.1	103.4	1.56
Wang et al.[81]	4	0	ASTM A131 EH36	L-PBF	-	M; P	891	4.21	99.3	76.1	1.70
Wang et al.[82]	4	0	ASTM A131 EH36	L-PBF	-	Edm; P	971	5.18	170.2	134.4	1.60
Wang et al.[82]	4	0	ASTM A131 EH36	L-PBF	-	Edm; P	921	5.49	146.4	119.0	1.51
Wang et al.[82]	4	0	ASTM A131 EH36	L-PBF	-	Edm; P	891	4.17	115.8	88.8	1.70
Okazaki[83]	6	90	Co-28Cr-6Mo	L-PBF	-	M	1156	8.86	293.4	260.5	1.27
, Wai Cho et al.[84]	8	90	CoCrMo	L-PBF	HT	P	1118	11.03	224.9	204.3	1.21
Wai Cho et al.[84]	10	90	CoCrMo	L-PBF	HT	P	1110	14.46	229.2	213.0	1.16
Kuzminova et al.[85]	4	90	CrFeCoNi	L-PBF	HT	B	638	12.38	159.5	154.2	1.07
Kuzminova et al.[85]	4	90	CrFeCoNi	L-PBF	NHT	M; P	658	4.21	196.7	181.3	1.18
Kuzminova et al.[85]	6	90	CrFeCoNi	L-PBF	HT	M; P	638	10.55	204.8	176.5	1.35
He et al.[86]	13	0	ER4043 aluminium	W-DED	-	M; P	164	4.75	28.4	22.4	1.62
He et al.[86]	8	0	ER4043 aluminium	W-DED	HT	M; P	147	11.30	41.1	38.0	1.17
Xie et al.[87]	18	0	ER5087 aluminium	W-DED	-	M	292	5.40	49.6	42.8	1.34
Shao et al.[88]	5	0	GH4169	P-DED	-		903	8.75	160.2	124.7	1.65

(continued)

Table 1. (Continued)

Ref.	N. of Data	Angle (°)	Material	Types of AM	Heat treatment	Surface operation	σ_{UTS} (MPa)	k 50	σ_{50} (MPa)	σ_{90} (MPa)	$T_{\sigma\,90}$
Han et al.[89]	15	90	Hastelloy-X	L-PBF	NHT	P	620	3.72	95.2	87.4	1.19
Poulin et al.[90]	10	90	IN625	L-PBF	HT	M; P	955	14.90	287.7	277.4	1.08
Balbaa et al.[58]	9	90	IN625	L-PBF	-	B	901	4.12	115.9	91.7	1.60
Balbaa et al.[58]	5	90	IN625	L-PBF	-	SP	901	11.56	237.6	228.6	1.08
Theriault et al.[91]	7	90	IN625	P-DED	HT	M; P	744	13.54	193.3	178.8	1.17
Theriault et al.[91]	9	90	IN625	P-DED	HT	M; P	697	10.09	190.8	181.1	1.11
Klein Fiorentin et al.[92]	9	0	IN625	P-DED	NHT	M	810	8.70	218.9	201.0	1.19
Sarkar et al.[93]	10	90	IN718	P-DED	HT	Edm; P	1134	5.94	162.2	139.4	1.35
Sarkar et al.[93]	13	90	IN718	P-DED	HT	Edm; P	1134	3.67	135.0	110.1	1.50
Wan et al.[94]	6	0	IN718	L-PBF	HT	Edm; G; P; EP	1451	3.48	152.0	122.8	1.53
Wan et al.[94]	10	0	IN718	L-PBF	HT	Edm; G; P; EP	1451	4.50	170.9	151.3	1.28
Wan et al.[94]	7	0	IN718	L-PBF	HT	Edm; G; P; EP	1451	5.89	201.3	181.6	1.23
Wan et al.[94]	8	0	IN718	L-PBF	HT	Edm; G; P; EP	1451	10.22	214.9	180.9	1.41
Sabelkin et al.[95]	4	0	IN718	L-PBF	NHT	B	986	4.05	99.5	77.4	1.65
Musekamp et al.[96]	9	90	Scalmalloy	L-PBF	HT	M	510	12.63	80.8	66.6	1.47
Musekamp et al.[96]	4	90	Scalmalloy	L-PBF	HT	B	510	5.05	35.7	29.3	1.49
Shin et al.[97]	8	90	SS420	B jetting	HT	Edm; M; P	656	6.71	147.4	133.0	1.23
Zhou et al.[98]	4	0	Ti-13Nb-13Zr	L-PBF	-	B	1064	5.83	73.7	65.0	1.29
Zhou et al.[98]	5	0	Ti-13Nb-13Zr	L-PBF	-	B	1106	4.89	85.6	66.6	1.65
Zhou et al.[98]	5	0	Ti-13Nb-13Zr	L-PBF	-	B	1085	5.59	86.6	69.0	1.58
Zhou et al.[98]	4	0	Ti-13Nb-13Zr	L-PBF	-	B	1053	5.43	78.3	66.8	1.37
Dietrich et al.[43]	10	0	Ti-6Al-4V	L-PBF	HT	M	1233	8.18	231.0	197.2	1.37
Dietrich et al.[43]	10	0	Ti-6Al-4V	L-PBF	HT	M	1203	8.95	245.5	210.1	1.36
Greitemeier et al.[18]	10	90	Ti-6Al-4V	E-PBF	HT	B	972	4.05	55.3	51.1	1.17
Greitemeier et al.[18]	10	90	Ti-6Al-4V	L-PBF	HT	B	1165	3.61	62.4	52.1	1.43
Greitemeier et al.[18]	9	90	Ti-6Al-4V	E-PBF	HT	M	972	4.22	90.4	73.0	1.54
Benedetti et al.[99]	7	90	Ti-6Al-4V	L-PBF	HT	B	1090	3.74	80.7	62.1	1.69
Biswal et al.[100]	8	90	Ti-6Al-4V	W-DED	-	M; P	859	13.33	303.3	286.6	1.12
Biswal et al.[100]	6	90	Ti-6Al-4V	W-DED	-	M; P	859	11.53	265.5	251.7	1.11
Biswal et al.[100]	18	90	Ti-6Al-4V	W-DED	-	M; P	842	4.68	135.5	104.9	1.67
Kahlin et al.[20]	7	90	Ti-6Al-4V	L-PBF	HT	LP	1108	3.18	47.4	39.9	1.41
Le et al.[101]	9	90	Ti-6Al-4V	L-PBF	HT	B	927	3.98	81.0	73.4	1.21
Le et al.[101]	12	90	Ti-6Al-4V	L-PBF	HT	B	927	4.32	88.0	78.7	1.25
Syed et al.[102]	12	0	Ti-6Al-4V	W-DED	NHT	P	951	8.41	269.1	230.3	1.37
Syed et al.[102]	12	90	Ti-6Al-4V	W-DED	NHT	P	898	9.90	278.6	240.2	1.34
Gong et al.[17]	6	90	Ti-6Al-4V	L-PBF	NHT	M	978	4.15	53.7	45.7	1.38
Franchitti et al.[103]	19	90	Ti-6Al-4V	E-PBF	NHT	M	1020	7.80	428.8	357.5	1.44
Franchitti et al.[103]	15	90	Ti-6Al-4V	E-PBF	NHT	B	919	4.47	112.4	86.2	1.70
Brika and Brailovski[104]	10	90	Ti-6Al-4V	L-PBF	HT	M	930	5.97	178.8	139.7	1.64
Brika and Brailovski[104]	10	90	Ti-6Al-4V	L-PBF	HT	M	1001	5.25	177.3	152.1	1.36
Wanjara et al.[105]	4	90	Ti-6Al-4V	E-PBF	-	B	1015	3.84	73.2	71.1	1.06
Wanjara et al.[105]	5	90	Ti-6Al-4V	E-PBF	-	B	981	4.03	54.1	49.9	1.18
Wanjara et al.[105]	5	90	Ti-6Al-4V	E-PBF	-	M	1045	4.20	63.3	55.9	1.28
Jimenez et al.[106]	8	90	Ti-6Al-4V	L-PBF	HT	M	879	6.48	197.7	172.0	1.32
Segurajauregi et al.[107]	6	90	Ti-6Al-4V	L-PBF	-	B	1159	3.08	38.8	33.9	1.31
Segurajauregi et al.[107]	7	90	Ti-6Al-4V	L-PBF	-	B	1115	3.60	44.4	41.0	1.17
Springer et al.[108]	19	0	Ti-6Al-4V	W-DED	NHT	M; P	957	4.39	132.2	101.7	1.69

B: as-built; M: machined; G: grind; P: polished; LP: laser polished; EP: electropolished; V: vibrofinish; S: sandblast; T: tribofinish.

equations (3) and (4), where x_m and y_m are the averages of the logarithm of life and stress values, respectively.

$$log(N_f) = c_0 + c_1.log(\sigma) \qquad (2)$$

$$c_1 = \frac{\sum_{i=1}^{number\ of\ data}[\log(\sigma_i) - x_m].[\log(N_{f,i}) - y_m]}{\sum_{i=1}^{number\ of\ data}[\log(\sigma_i) - x_m]^2} \qquad (3)$$

$$c_0 = y_m - c_1.x_m \qquad (4)$$

The negative value of c_1 gives the negative inverse slope (k) which is an essential parameter in the calculation of endurance limit $\sigma_{A,50\%}$ for $P_s = 50\%$. Equation (2) is written in a simple form as equation (5) to make clear the calculation of the endurance limit.

$$\sigma_{A,50\%} = \left(\frac{10^{c_0}}{N_A}\right)^{1/k} \qquad (5)$$

Although the fatigue data for additively manufactured metals were compared by using $\sigma_{A,50\%}$ in this study,

Table 2. Summary of the re-analysed data for -1 loading ratio.

Ref.	N. of Data	Angle (°)	Material	Types of AM	Heat-treatment	Surface operation	σ_{UTS} (MPa)	k_{50}	σ_{50} (MPa)	σ_{90} (MPa)	$T_{\sigma\,90}$
Nezhadfar et al.[109]	9	90	17-4 PH	L-PBF	HT	M; P	1238	6.91	423.7	365.8	1.34
Nezhadfar et al.[109]	7	90	17-4 PH	L-PBF	HT	M; P	1192	7.66	467.1	400.1	1.36
Yadollahi et al.[26]	8	90	17-4 PH	L-PBF	NHT	M; P	940	6.44	197.2	156.1	1.60
Yadollahi et al.[26]	9	0	17-4 PH	L-PBF	NHT	M; P	1060	7.12	263.7	212.5	1.54
Carneiro et al.[110]	18	90	17-4 PH	L-PBF	HT	B	1110	5.75	271.0	205.2	1.74
Nezhadfar et al.[47]	8	0	17-4 PH	L-PBF	HT	B	1117	3.83	119.7	105.2	1.29
Nezhadfar et al.[47]	7	90	17-4 PH	L-PBF	HT	M	1117	5.52	333.6	304.8	1.20
Nezhadfar et al.[47]	9	90	17-4 PH	L-PBF	HT	B	1132	3.34	120.0	102.5	1.37
Nezhadfar et al.[47]	6	90	17-4 PH	L-PBF	HT	M; P	1132	4.03	282.4	246.3	1.31
Nezhadfar et al.[47]	6	90	17-4 PH	L-PBF	HT	B	1167	4.04	182.4	150.0	1.48
Nezhadfar et al.[47]	6	90	17-4 PH	L-PBF	HT	M; P	1167	7.65	441.2	372.7	1.40
Nezhadfar et al.[47]	9	90	17-4 PH	L-PBF	HT	B	1375	3.47	147.9	112.5	1.73
Nezhadfar et al.[47]	5	90	17-4 PH	L-PBF	HT	M; P	1375	5.42	368.2	355.8	1.07
Nezhadfar et al.[47]	6	90	17-4 PH	L-PBF	HT	M; P	948	6.94	401.5	339.5	1.40
Molaei et al.[111]	4	90	17-4 PH	L-PBF	HT	P	1193	6.50	348.5	270.8	1.66
Molaei et al.[111]	6	90	17-4 PH	L-PBF	HT	M	1193	7.92	460.0	397.3	1.34
Yadollahi et al.[112]	12	90	17-4 PH	L-PBF	HT	M; P	1150	4.58	148.5	115.3	1.66
Damon et al.[113]	16	0	18Ni300	L-PBF	HT	M; P	1926	3.63	199.8	168.8	1.40
Elangeswaran et al.[114]	20	90	18Ni300	L-PBF	NHT	B	1176	2.85	102.9	79.1	1.69
Elangeswaran et al.[114]	14	90	18Ni300	L-PBF	HT	S	1744	9.26	644.5	568.2	1.29
Elangeswaran et al.[114]	11	90	18Ni300	L-PBF	NHT	V	1176	9.70	479.5	441.9	1.18
Elangeswaran et al.[114]	11	90	18Ni300	L-PBF	NHT	S	1176	9.05	422.9	369.8	1.31
Elangeswaran et al.[114]	12	90	18Ni300	L-PBF	HT	B	1744	2.47	73.9	63.4	1.36
Elangeswaran et al.[114]	8	90	18Ni300	L-PBF	HT	V	1744	7.02	488.9	381.0	1.65
Cutolo et al.[34]	11	90	316L	L-PBF	NHT	B	573	4.63	142.4	130.7	1.19
Cutolo et al.[34]	10	90	316L	L-PBF	HT	B	570	3.73	123.0	109.2	1.27
Lai et al.[115]	6	90	316L	L-PBF	HT	P	601	5.40	200.0	174.5	1.31
Lai et al.[115]	6	90	316L	L-PBF	NHT	P	633	3.25	119.4	112.4	1.13
Elangeswaran et al.[116]	12	90	316L	L-PBF	NHT	B	573	4.60	142.3	131.4	1.17
Elangeswaran et al.[116]	10	90	316L	L-PBF	HT	B	570	3.71	122.7	109.0	1.27
Afkhami et al.[64]	4	0	316L	L-PBF	NHT	Edm; G	723	7.45	245.6	227.6	1.16
Elangeswaran et al.[117]	11	90	316L	L-PBF	NHT	B	573	4.63	142.4	130.9	1.18
Elangeswaran et al.[117]	10	90	316L	L-PBF	HT	B	570	3.71	122.7	108.8	1.27
Blinn et al.[118]	10	0	316L	L-PBF	-	M; P	678	12.85	317.7	306.1	1.08
Blinn et al.[119]	9	0	316L	L-PBF	HT	B	681	4.74	172.4	141.4	1.49
Blinn et al.[119]	11	90	316L	L-PBF	HT	B	600	3.36	106.4	92.5	1.32
Kotzem et al.[120]	4	0	316L	L-PBF	-	M; P	685	11.87	297.4	230.6	1.66
Kotzem et al.[120]	5	0	316L	L-PBF	-	M; P	596	10.88	240.2	214.9	1.25
Yu et al.[121]	14	0	316L	L-PBF	-	Edm; EP	681	5.12	205.1	161.6	1.61
Yu et al.[121]	12	0	316L	L-PBF	-	Edm; EP	706	4.49	185.2	157.2	1.39
Blinn et al.[3]	13	90	316L	L-PBF	-	M; P	612	4.89	134.1	101.6	1.74
Blinn et al.[3]	10	90	316L	P-DED	-	M; P	564	6.27	137.1	106.5	1.66
Blinn et al.[3]	10	0	316L	L-PBF	-	M; P	681	6.34	205.2	171.5	1.43
Blinn et al.[3]	9	0	316L	P-DED	-	M; P	629	11.52	222.6	191.4	1.35
Uematsu et al.[122]	6	0	420J1 SS	P-DED	-	M; P	1737	7.47	477.2	392.9	1.47
Nezhadfar et al.[24]	6	90	AlF357	L-PBF	HT	M	390	6.80	97.8	85.5	1.31
Nezhadfar et al.[24]	6	0	AlF357	L-PBF	HT	M	370	5.08	70.3	53.9	1.70
Lai et al.[40]	7	90	AlSi10Mg	L-PBF	HT	P	251	14.86	82.1	73.1	1.26
Nezhadfar et al.[24]	5	90	AlSi10Mg	L-PBF	HT	M	350	14.41	116.7	108.2	1.16
Nezhadfar et al.[24]	6	0	AlSi10Mg	L-PBF	HT	M	340	9.96	103.3	93.7	1.22
Romano et al.[123]	10	0	AlSi10Mg	L-PBF	NHT	M	442	3.79	55.7	46.3	1.44
Zhang et al.[124]	4	90	AlSi10Mg	L-PBF	NHT	M	478	5.03	79.0	68.6	1.33
Domfang Ngnekou et al.[125]	14	0	AlSi10Mg	L-PBF	HT	M	338	6.00	84.7	68.6	1.53
Domfang Ngnekou et al.[125]	4	90	AlSi10Mg	L-PBF	HT	M	350	11.88	91.4	84.0	1.18
Domfang Ngnekou et al.[125]	7	0	AlSi10Mg	L-PBF	HT	M	328	7.59	81.4	75.4	1.17
Muhammad et al.[126]	6	90	AlSi10Mg	L-PBF	HT	B	302	4.59	52.2	44.3	1.39
Muhammad et al.[126]	6	90	AlSi10Mg	L-PBF	HT	B	366	4.84	58.3	48.5	1.45
Muhammad et al.[126]	5	90	AlSi10Mg	L-PBF	HT	M	302	8.25	91.6	86.3	1.13
Muhammad et al.[126]	7	90	AlSi10Mg	L-PBF	HT	M	366	7.82	104.7	97.2	1.16
Sausto et al.[127]	13	90	AlSi10Mg	L-PBF	HT	B	382	3.39	33.0	29.2	1.27
Awd et al.[128]	4	0	AlSi10Mg	L-PBF	NHT	M; G; P	380	12.13	106.5	84.5	1.59
Awd et al.[128]	4	90	AlSi10Mg	L-PBF	NHT	M; G; P	352	3.31	46.2	40.0	1.33
Yamashita et al.[129]	4	0	IN718	L-PBF	HT	M; P	1467	4.55	286.8	219.4	1.71

(continued)

Table 2. (Continued)

Ref.	N. of Data	Angle (°)	Material	Types of AM	Heat-treatment	Surface operation	σ_{UTS} (MPa)	k_{50}	σ_{50} (MPa)	σ_{90} (MPa)	$T_{\sigma\,90}$
Liu et al.[130]	4	0	IN718	L-PBF	NHT	M; EP	1176	6.82	277.0	240.4	1.33
Liu et al.[130]	9	0	IN718	L-PBF	HT	M; EP	1593	3.19	202.5	154.5	1.72
Yu et al.[131]	11	0	IN718	P-DED	HT	M	1309	4.95	327.7	277.1	1.40
Nishikawa et al.[7]	4	90	IN718	L-PBF	HT	M; P	1350	9.83	549.8	487.5	1.27
Nishikawa et al.[7]	4	90	IN718	L-PBF	HT	M; P	1350	5.24	366.2	329.0	1.24
Nishikawa et al.[7]	4	90	IN718	E-PBF	HT	M; P	1240	3.32	188.5	152.3	1.53
Doh et al.[132]	12	0	Maraging Steel	L-PBF	NHT	B	1150	4.02	163.2	129.3	1.59
Doh et al.[132]	13	0	Maraging Steel	L-PBF	NHT	M	1150	4.92	263.8	201.9	1.71
Doh et al.[132]	14	0	Maraging Steel	L-PBF	HT	M	2037	3.75	258.2	198.8	1.69
Meneghetti et al.[133]	9	90	Maraging Steel	L-PBF	NHT	P	1217	3.61	88.9	72.5	1.50
Meneghetti et al.[133]	9	90	Maraging Steel	L-PBF	HT	P	2034	3.92	132.4	102.3	1.68
Meneghetti et al.[133]	9	0	Maraging Steel	L-PBF	NHT	P	1203	5.99	192.7	147.5	1.71
Nezhadfar et al.[24]	4	90	QuesTek Al	L-PBF	HT	M	496	5.76	110.5	95.5	1.34
Muhammad et al.[126]	8	90	QuesTek Al	L-PBF	HT	B	496	2.92	23.9	18.6	1.64
Muhammad et al.[126]	6	90	QuesTek Al	L-PBF	HT	M	496	4.76	87.1	66.4	1.72
Wei et al.[134]	10	0	Ti-5Al-2.5Sn	L-PBF	-	M	1167	7.61	362.5	315.8	1.32
Cutolo et al.[34]	8	90	Ti-6Al-4V	L-PBF	HT	B	1002	6.78	195.8	180.0	1.18
Cutolo et al.[34]	10	90	Ti-6Al-4V	L-PBF	NHT	B	1246	2.95	57.2	48.7	1.38
Kaya et al.[135]	6	0	Ti-6Al-4V	E-PBF	NHT	M	990	7.23	247.3	199.3	1.54
Bhandari and Gaur[136]	10	0	Ti-6Al-4V	L-PBF	HT	B	948	5.88	207.3	167.5	1.53
Benedetti et al.[99]	11	90	Ti-6Al-4V	L-PBF	HT	B	1090	3.92	142.4	113.0	1.59
Benedetti et al.[99]	9	90	Ti-6Al-4V	L-PBF	HT	B	950	11.27	177.1	149.5	1.40
Benedetti et al.[99]	6	90	Ti-6Al-4V	L-PBF	HT	EP	1090	7.85	247.5	203.8	1.48
Benedetti et al.[99]	8	90	Ti-6Al-4V	L-PBF	HT	T	960	5.39	259.6	226.4	1.31
Sun et al.[28]	15	0	Ti-6Al-4V	L-PBF	HT	M	936	4.90	207.9	167.5	1.54
Sun et al.[28]	19	90	Ti-6Al-4V	L-PBF	HT	M	953	9.57	384.9	336.6	1.31
Karimi et al.[137]	12	90	Ti-6Al-4V	L-PBF	HT	M	1043	2.98	63.4	53.1	1.43
Singla et al.[138]	7	90	Ti-6Al-4V	L-PBF	HT	M	1228	6.87	311.5	248.7	1.57
Singla et al.[138]	4	90	Ti-6Al-4V	L-PBF	NHT	M	1315	3.22	144.4	122.1	1.40
Singla et al.[138]	5	90	Ti-6Al-4V	L-PBF	HT	M	986	3.24	128.6	102.6	1.57
Fousová et al.[16]	12	90	Ti-6Al-4V	E-PBF	NHT	B	1132	3.42	110.1	93.6	1.38
Fousová et al.[16]	10	90	Ti-6Al-4V	L-PBF	HT	B	1045	5.50	194.5	172.0	1.28
Williams et al.[139]	9	0	WE43	AFSD	-	Edm; P	264	9.87	95.9	80.8	1.41
Williams et al.[139]	7	90	WE43	AFSD	-	Edm; P	224	10.94	89.9	80.1	1.26

B: as-built; M: machined; G: grind; P: polished; EP: electropolished; V: vibrofinish; S: sandblast; T: tribofinish; AFSD: additive friction stir deposition.

one can calculate the scatter band of the data in the desired confidence level by using equations (6) and (7) with the help of q values and the formulation of the standard deviation (s) in equation (8). q values are a statistical index related to confidence level, and they are available in the literature.[141] The results of the statistical re-analysis are given in Tables 1 and 2.

$$\sigma_{A,P\%} = \sigma_{A,50\%}\left(\frac{N_A}{10^{\log(N_A)+q.s}}\right)^{1/k} \qquad (6)$$

$$\sigma_{A,(1-P)\%} = \sigma_{A,50\%}\left(\frac{N_A}{10^{\log(N_A)-q.s}}\right)^{1/k} \qquad (7)$$

$$s = \left(\frac{\sum_1^{number\ of\ data}\left(\log(N_{f,i}) - \log\left(N_A\left(\frac{\sigma_{A,50\%}}{\sigma_i}\right)^k\right)\right)^2}{number\ of\ data - 1}\right)^{0.5} \qquad (8)$$

Statistical re-analysis results

To investigate whether any relationships were readily apparent from the re-analysed fatigue data the calculated values of $\sigma_{A,50\%}$ and k were plotted against the material ultimate tensile strength (UTS). Figures 1 and 2 show representative examples of these plots for data sets with a load ratio of 0.1 differentiated by material and surface operations. Note that the $0.25 \times \sigma_{UTS}$ line included in Figure 1 is provided as a reference and is not a best-fit line. Examination of these plots for different combinations of variables showed no clear trends or relationships. Although the data obtained was scattered, many of the endurance limit data were smaller than the 0.25 of their ultimate stress value for both $R = -1$ and 0.1, independent from the material types and specimen direction. Additionally, 59% of the k values were between 3 and 6 for $R = -1$ and 0.1.
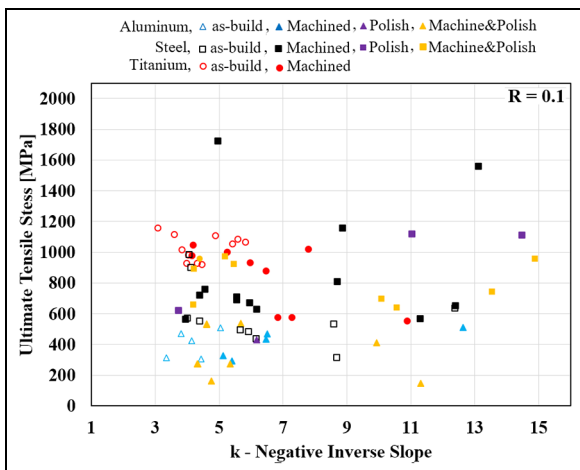
Mean stress effect at the endurance limit

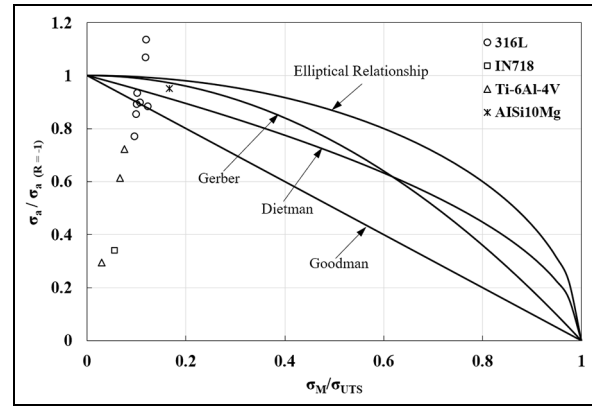The effect of non-zero mean stress on fatigue life was investigated for the non-heat-treated 3D-printed
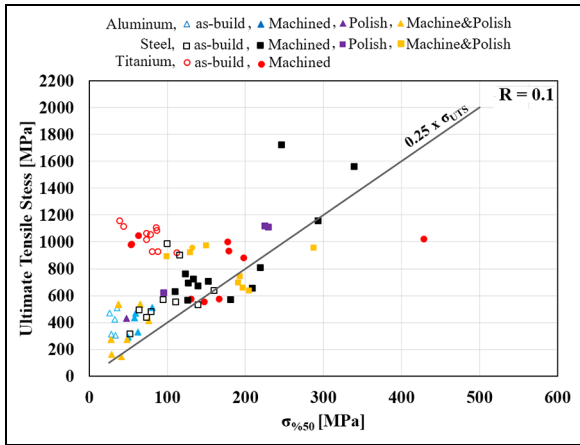
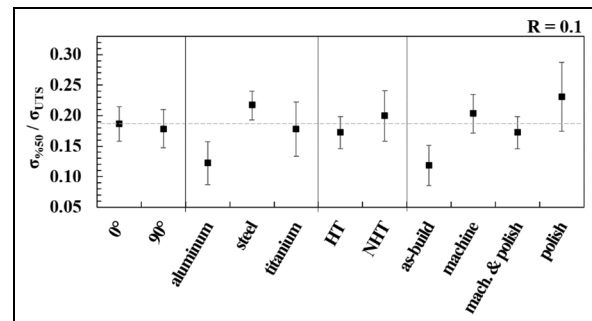**Figure 1.** Effect of surface operations on endurance limit, R = 0.1.

Figure 2. Effect of surface operations on *k*-negative inverse slope, R = 0.1.

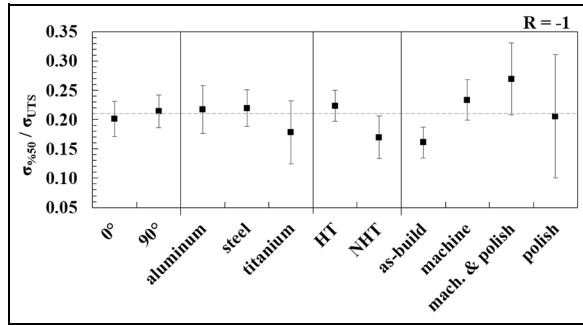**Figure 3.** Effect of non-zero mean stresses at endurance limit on fatigue.

Figure 4. Mean and intervals of data for $\sigma_{\%50}/\sigma_{UTS}$, R = 0.1.

Main and interaction effect analysis

The graphs used to investigate the effect of different parameters in the previous section were scattered, so making a deduction with these graphs was not straightforward. To investigate whether any parameters (main effect), or pairs of parameters (interaction effect), had a significant influence on the endurance limit or negative inverse slope the mean values and 95% confidence intervals for all data corresponding to a given parameter were calculated and compared. To enable cross-material comparison the endurance limit was normalised by the material UTS. The main effect and interaction effect analyses of the mentioned parameters for endurance limit and negative inverse slope are given in the next subsections.

Main effect analyses for endurance limit

The main effect analyses were performed for stress ratios $R = -1$ and 0.1, and the results are given separately. The results were calculated for specimen build direction, material, heat treatment and surface operations separately. The endurance limit values were normalised by ultimate tensile stress in Figures 4 and 5 and the intervals shown are the 95% confidence

materials. The endurance limit data for four different materials were used to generate the graph in Figure 3. Stress amplitudes at the endurance limit was obtained for different loading ratios and normalised by the stress amplitude at the endurance limit under $R = -1$ loading ratio. The mean stresses were normalised by the ultimate tensile stress of each material in the condition of as-built and non-heat-treated. Also included in Figure 3 are the expressions of Goodman, Gerber, Dietman and the elliptical relationship that are known to analyse the effect of non-zero mean stresses on fatigue are used to compare the experimental results in a non-dimensional way. All the titanium data plotted in Figure 3 fall within the Goodman curve, whilst the only aluminium data point lies above the Goodmand and Dietman curves but below the Gerber and Elliptical curves. Two 316L data points fall above all four curves with the remaining 6 points clustered close to the Goodman curve.

Figure 5. Mean and intervals of data for $\sigma_{\%50}/\sigma_{UTS}$, $R = -1$.

intervals. The number of data corresponding to each specimen condition for stress ratios $R = -1$ and 0.1 are given in Tables 3 and 4, respectively. Taking a coarse view, using all data without any classification, the mean $\sigma_{\%50}/\sigma_{UTS}$ values were 0.18 and 0.21 for $R = 0.1$ and $R = -1$, respectively.

Suppose only the specimen direction is filtered and the changes in other parameters are not taken into account; the mean value is around 0.2 for both

specimen directions, 0° and 90° under for $R = 0.1$ and $R = -1$, separately. The intervals of the means are seen on the graphs, and it is acceptable. So, one can select $\sigma_{\%50}/\sigma_{UTS}$ value from the upper or below limits of intervals according to conservation level. On the other hand, by comparing the mean values between 0° and 90°, any effect of specimen directions on the endurance limit is not seen on results. The mean values for different material types, heat treatments, surface operations and their intervals are also given in the figures. Due to the main stress effect under $R = 0.1$, the endurance limit of the material is expected to be lower than $R = -1$, and it is generally seen to be so by comparison of the graphs. However, this is not clear since the number of data and their scatter band are not similar between two stress ratios. Although a relationship cannot be seen clearly in Figures 4 and 5 with the changes of specimen directions, material types, or heat treatment on $\sigma_{\%50}/\sigma_{UTS}$, it does increase with the effect of surface operations from as-built to machine & polishing. Since a small number of data are available for only polished materials, the interval of the data is very high and, its

Table 3. Mean analyses of σ_{50}/σ_{UTS} for R = 0.1, −1 and used numbers of data.

Parameters	σ_{50}/σ_{UTS} ; R = 0.1					σ_{50}/σ_{UTS} ; R = −1				
	Mean	Std. dev.	95% CI upper	Max. Z-score	N	Mean	Std. dev.	95% CI upper	Max. Z-score	N
0°	0.1865	0.063	0.2146	−1.75	19	0.2015	0.060	0.2293	1.70	18
90°	0.1784	0.095	0.2098	2.55	35	0.2139	0.103	0.2412	1.72	55
aluminium	0.1219	0.062	0.1571	2.54	12	0.2173	0.082	0.2553	−2.05	18
steel	0.2168	0.056	0.2403	−2.05	22	0.2192	0.099	0.2496	2.05	41
titanium	0.1779	0.102	0.2224	2.38	20	0.1779	0.093	0.2267	2.42	14
HT	0.1720	0.081	0.1985	1.84	36	0.2234	0.098	0.2490	2.05	56
NHT	0.1998	0.090	0.2413	−1.61	18	0.1694	0.071	0.2029	−1.74	17
as-build	0.1185	0.065	0.1513	2.2	15	0.1608	0.068	0.1863	−1.70	27
machine	0.2032	0.074	0.2349	2.93	21	0.2336	0.084	0.2666	−2.05	25
mach.&polish	0.1720	0.081	0.1984	1.84	13	0.2693	0.106	0.3248	−1.56	14
polish	0.2309	0.064	0.2871	1.23	5	0.2056	0.114	0.2901	−1.23	7
Mean	0.18					0.21				

Table 4. Mean analyses of k for R = 0.1, −1 and used numbers of data.

| Parameters	k ; R = 0.1					k ; R = −1				
	Mean	Std. dev.	95% CI upper	Max. Z-score	N	Mean	Std. dev.	95% CI upper	Max. Z-score	N
0°	6.349	2.035	7.264	2.43	19	5.440	1.673	6.213	2.70	18
90°	6.967	3.582	8.153	2.21	35	5.287	2.200	5.880	2.98	53
aluminium	6.026	2.932	7.685	1.80	12	7.096	3.575	8.748	2.17	18
steel	7.694	3.718	9.248	1.93	22	4.802	1.438	5.248	2.16	40
titanium	6.144	2.263	7.135	2.09	20	5.552	2.583	6.906	2.21	14
HT	7.307	3.454	8.435	2.19	36	5.540	2.209	6.135	2.87	53
NHT	5.634	1.947	6.533	2.18	18	4.571	1.408	5.240	1.80	17
as-build	4.239	0.660	4.598	−1.35	13	4.119	1.040	4.518	2.56	26
machine	6.720	2.232	7.674	2.64	21	6.488	2.790	7.581	1.93	25
mach. & polish	7.672	3.904	9.795	1.85	13	5.952	1.860	6.926	−1.41	14
polish	9.505	3.928	12.94	−1.47	5	6.217	4.009	9.187	2.16	7
Mean	6.75					5.55				
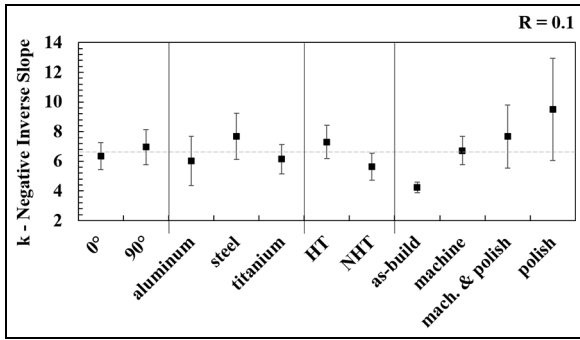
Figure 6. Mean and intervals of *k* values, R = 0.1.
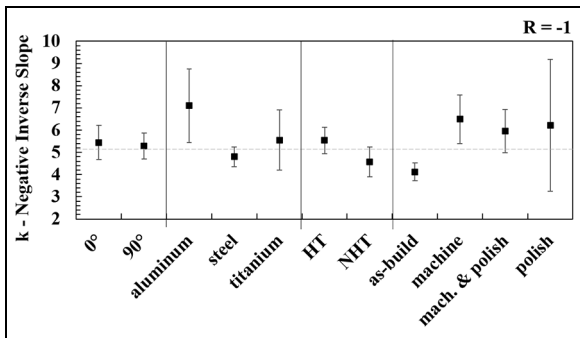

Figure 7. Mean and intervals of *k* values, R = −1.

mean value breaks the trend for the relation between $\sigma_{\%50}/\sigma_{UTS}$ and surface operations.

Main effect analyses for negative inverse slope (k)

The main effect analyses for the negative inverse slope, (*k*) values were performed for stress ratios

$R = -1$ and 0.1, and the results are given separately. The results were calculated independently for specimen direction, materials, heat treatments and surface operations. Without any classification of data, the mean values of the negative inverse slope were obtained as 6.7 and 5.5 for 0.1 and −1 loading ratios, respectively. So, the endurance limit could be estimated by using only the negative inverse slope written above and ultimate tensile stress values independent from manufacturing direction, material type, or post-processing history of the 3D-printed metals. In Figures 6 and 7, mean and interval values can be seen for selected parameters independently.

Interaction effects analyses for endurance limit and negative inverse slope (k)

In this subsection, the interaction of parameters and their effects on the endurance limit and negative inverse slope are investigated. In Figures 8 to 11, each line (in order from top to bottom) shows the effect of interactions of parameters with specimen build direction, material type and heat treatment on $\sigma_{\%50}/\sigma_{UTS}$ or *k*. The results are given at the right-side of the graph for $\sigma_{\%50}/\sigma_{UTS}$ in Figures 8 and 9 for R = 0.1 and −1, respectively. The symbols and the colours of the parameters are seen on graphs. The material types are given with the first letters for Aluminium, Steel and Titanium. All values on the graphs are independent. The individual effect of surface operations on $\sigma_{\%50}/\sigma_{UTS}$ and negative inverse slope (*k*) can be seen in the right column of the graphs. It is also mentioned in the previous section. Except this, any effect of the parameters on $\sigma_{\%50}/\sigma_{UTS}$ or negative inverse slope (*k*) cannot be observed from the interaction graphs.
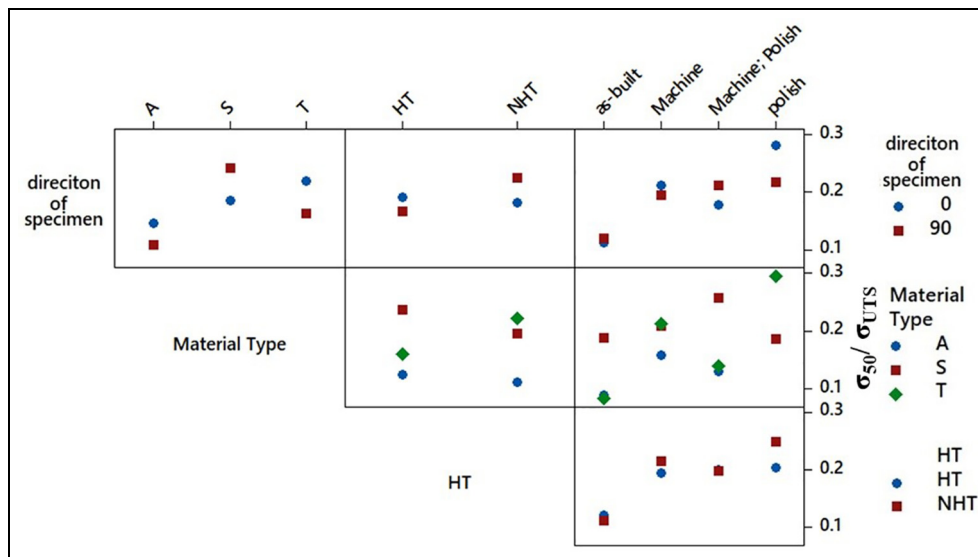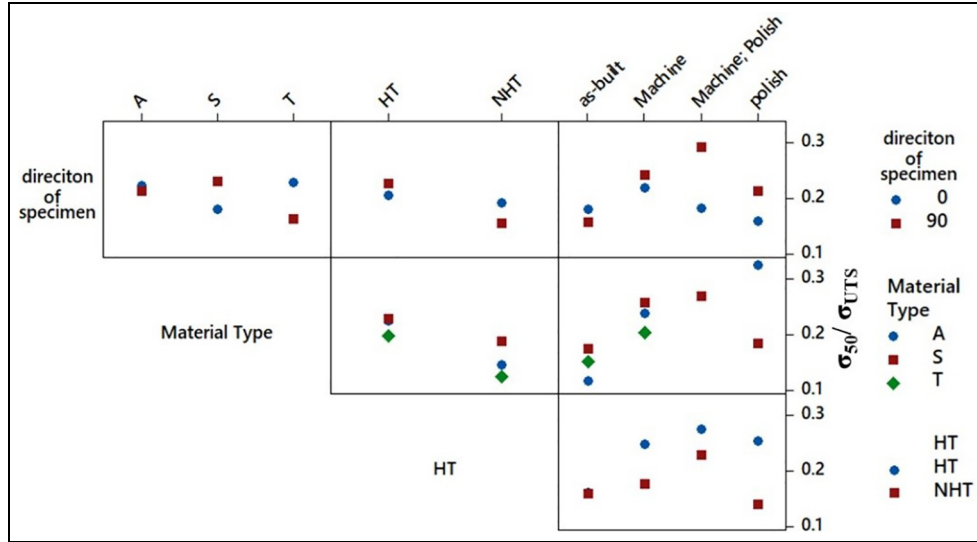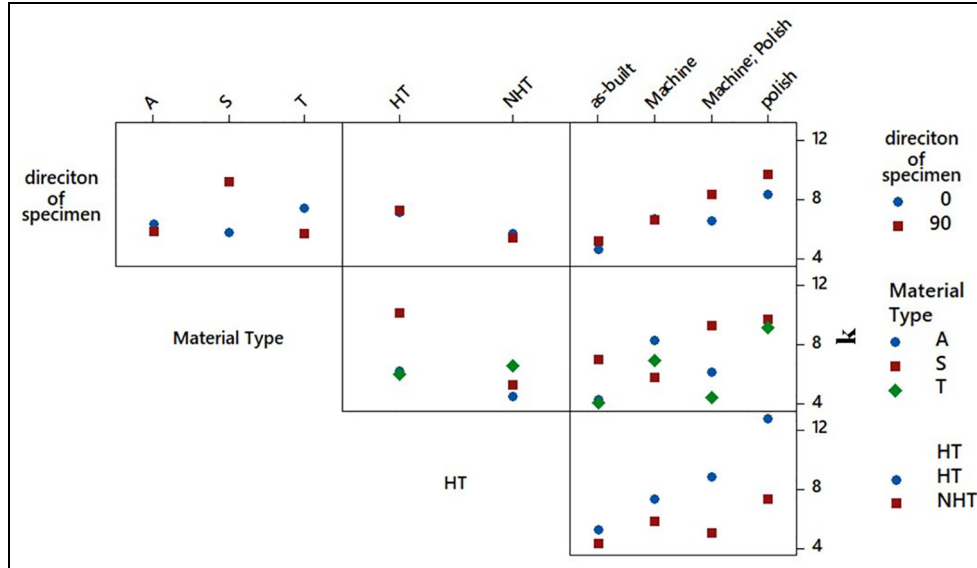

Figure 8. Interaction plots of $\sigma_{A,50}/\sigma_{UTS}$ for R = 0.1.

Figure 9. Interaction plots of $\sigma_{A,50}/\sigma_{UTS}$ for $R = -1$.

Figure 10. Interaction plots of negative inverse slope (k) for $R = 0.1$.

## Multiple linear regression sensitivity analysis

To further test for variables, or combinations of variables, which had a significant effect on the normalised high-cycle fatigue reference value, σ_{50}/σ_{UTS}, or fatigue curve negative inverse slope, k_{50}, a multiple linear regression analysis was used.

Multiple linear regression model and t-tests

Two multiple linear regression models with first-order interaction terms were fitted to the data set for each material using the software Minitab,[142] resulting in 6 regression models of the form:

$$y = \beta_0 + \beta_1 x_1 + \beta_2 x_2 + \cdots + \beta_6 x_6 + \beta_{1,2} x_1 x_2$$
$$+ \beta_{1,3} x_1 x_3 + \cdots + \beta_{3,6} x_3 x_6$$

In these multiple linear models y was either σ_{50}/σ_{UTS} or k_{50} and x_i were qualitative variables, which could only take the values 0 or 1, corresponding to the specimen and test conditions listed in Table 5. For example, to avoid model being confounded, for a σ_{50}/σ_{UTS} or k_{50} value corresponding to as-built samples $x_4, x_5, x_6 = 0$. The first-order interaction terms were included in the models to explore the possibility that combinations of variables had a more significant effect than individual variables. The coefficients in the above multiple linear models correspond to variables,
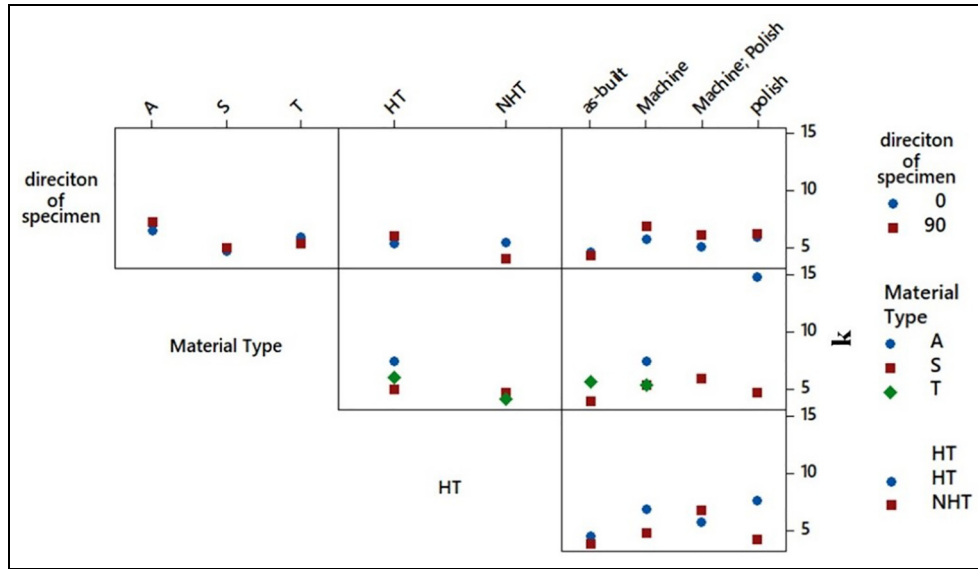
Figure 11. Interaction plots of negative inverse slope (k) for $R = -1$.

Table 5. Explanatory variables used in the multiple linear regression models.

Condition group	Condition	Variable
Load ratio	$R = -1$	$x_1 = 0$
	$R = 0.1$	$x_1 = 1$
Build direction	$0°$	$x_2 = 0$
	$90°$	$x_2 = 1$
Heat treatment	Heat treated	$x_3 = 0$
	Not heat treated	$x_3 = 1$
Surface finish	As-built	$x_4, x_5, x_6 = 0$
	Machined	$x_4 = 1$
	Machined and polished	$x_5 = 1$
Polished		$x_6 = 1$

Table 6. R^2 value calculated for each second-order interaction linear regression model.

Material	Regression model	R^2 (%)
Aluminium	σ_{50}/σ_{UTS}	42.9
	k_{50}	20.7
Steel	σ_{50}/σ_{UTS}	27.2
	k_{50}	38.2
Titanium	σ_{50}/σ_{UTS}	27.2
	k_{50}	38.6

so β_2 is the main effect of x_2, whilst $\beta_{3,6}$ is the interaction effect of x_3 and x_6.

To test the prediction effectiveness of each regression model, the R^2 value was calculated. To test whether a relationship could exist between σ_{50}/σ_{UTS} or k_{50} and one, or a pair, of the explanatory variables t-statistic significance tests were performed on each coefficient in each model to test the hypothesis that the coefficient was equal to zero.[143] Tests were

Table 7. Coefficients for the aluminium second-order interaction linear regression models with a significance of 90% or greater for either the σ_{50}/σ_{UTS} or k_{50} model.

Model coefficient	Aluminium specimen condition	Significance	
		σ_{50}/σ_{UTS} (%)	k_{50} (%)
β_2	Build direction	92.1	86.5
β_4	Surface finish, machined	97.1	81.4
β_5	Surface finish, machined and polished	93.9	61.8
$\beta_{1,3}$	Load ratio + Heat treatment	99.9	63.6

conducted at a 90% level. If a test was passed, this indicated that a relationship between σ_{50}/σ_{UTS} or k_{50} and the variable, or pair of variables and might exist.

Multiple linear regression sensitivity results

The low R^2 values in Table 6 calculated for all 6 models show they are not suitable for predicting σ_{50}/σ_{UTS} and k_{50}. Several coefficients in the multiple linear regression models passed the significance test at a 90% threshold (see Tables 7–9). Passing this test indicates that a relationship exists between the explanatory variable and predicted variable (i.e. σ_{50}/σ_{UTS} or k_{50}), but it does not mean that the relationship is appropriate for prediction.[144] The way the variables were set up in the models means that if a relationship exists it represents a difference from the condition where all $x_i = 0$. In terms of the effect on fatigue strength, variables that passed the test for only the σ_{50}/σ_{UTS} model must have an equal effect on fatigue strength across all fatigue lives, whereas, variables

Table 8. Coefficients for the steel second-order interaction linear regression models with a significance of 90% or greater for either the σ_{50}/σ_{UTS} or k_{50} model.

Model coefficient	Steel specimen condition	Significance	
		σ_{50}/σ_{UTS} (%)	k_{50} (%)
	Surface finish, machined	83.9	98.2
$\beta_{1,3}$	Load ratio + Heat treatment	32.8	95.3
$\beta_{1,4}$	Load ratio + Surface finish, machined	67.3	97.2

Table 9. Coefficients for the titanium second-order interaction linear regression models with a significance of 90% or greater for either the σ_{50}/σ_{UTS} or k_{50} model.

Model coefficient	Titanium specimen condition	Significance	
		σ_{50}/σ_{UTS} (%)	k_{50} (%)
β_4	Surface finish, machined	99.9	53.5
β_5	Surface finish, machined and polished	97.0	100.0
$\beta_{1,6}$	Load ratio + Surface finish, polished	99.4	85.6
$\beta_{2,5}$	Build direction + Surface finish, machined and polished	85.0	100.0

that passed the test for only the k_{50} model must only affect fatigue strength at shorter fatigue lives. The poor prediction effectiveness of the models means it is not possible to state with certainty whether the effect of a variable is to improve or reduce fatigue strength.

For the aluminium data, only coefficients in the σ_{50}/σ_{UTS} model passed the significance test, indicating that the effects corresponding to these test conditions occurred across the full range of fatigue lives tested. Conversely, for the steel data only coefficients in the k_{50} model passed the significance test, so the effects were likely limited to shorter fatigue lives. Both titanium models had some significant coefficients making interpretation in this way more difficult.

The significance results indicate that a machined surface finish has an effect on fatigue strength, relative to the as-built surface, for all three metals. Aluminium and titanium were also sensitive to a machined and polished surface finish, whereas steel was not. Aluminium was the only metal to show sensitivity to the build direction independently of other test conditions. Interestingly, titanium showed sensitivity to build direction only when the specimen surface was machined and polished. Steel showed no significant sensitivity to build direction. Load ratio only appeared as a significant factor in combination with either heat treatment or surface finish for all three metals.

Prediction of fatigue curves using artificial intelligence

In this section, the effect of variables on the endurance limit and negative inverse slope is investigated using artificial intelligence algorithms. The database described in the previous sections was used. Considered machine learning algorithms in this study were Decision Tree, Support Vector Machines, K-Nearest Neighbour, Multi-Layer Perceptron, Partial Least Squares, Gaussian Process regression algorithms that are widely used in the literature.

Decision tree (DT)[145] algorithm is one of the most commonly used algorithm for classification in the machine learning studies. Categorical and continuous variables can be used in this algorithm. A model like a tree is created in this algorithm. The classification starts from the root. The impurity status of the feature, determined by the Gini index or entropy values, indicates a degree of inhomogeneity of the values. Since the feature with the highest impurity value provides the most information gain, the feature selection process is completed by selecting the feature with the highest impurity value. After selecting a feature to branch on, the decision tree establishes criteria by comparing numbers. The tree then branches based on the significance of these comparisons. When a branch reaches a fully classified, the branch is considered complete.

Support vector machines (SVM)[146] is another widely used algorithm in machine learning. Essentially, it determines an optimal boundary line that gives the maximum distances between classes. When it separates the data into two classes, the boundary line is linear. If more separations are needed to better classify the data, it uses a hyperplane that uses high-sized kernels. The support vectors are the data points that are closest to the hyperplane and have the most significant influence on the determination of the position of the hyperplane.

k-Nearest Neighbours (KNN)[147] is a versatile machine learning algorithm. It is a non-parametric learning algorithm, and it can be used for both classification and regression. A critical parameter affecting the model's sensitivity to noise is the determination of 'k', which represents the number of neighbours considered.

Multi-layer Perceptron (MLP)[148] is an essential type of artificial neural network. A multi-layer perceptron (MLP) consists of three basic layers: the input layer, the hidden layers and the output layer. Each layer includes neurons, and the neurons are connected to each other. Machine learning is achieved by using the weights between the neurons in each layer. Each neuron typically uses an activation function, such as a sigmoid, hyperbolic tangent or linear unit, which

allows the learning of complex relationships between layers. MLP allows data to be displayed hierarchically due to its multi-layer structure.

Partial Least Squares (PLS) regression,[149] which is based on statistical methods, is a commonly used method in the context of multivariate analysis and predictive modelling. The purpose of PLS regression is to define a linear relationship between the independent variables (features) and the dependent variables (responses) in a data set. It can be effective for data sets with a high number of variables, multicollinearity, or situations.

Gaussian Process Regression (GPR)[150,151] is a machine learning technique suitable for situations with unknown or complex relationships between input and output variables. This model uses kernel functions like the Radial Basis Function (RBF) kernel to determine the similarity between data points and provide predictions and associated uncertainties. Training the model requires a dataset of input-output pairs, and the posterior distribution over functions is computed using Bayes' rule. GPR has several benefits over other regression techniques, such as handling noisy data, incorporating prior knowledge about the problem and providing uncertainty estimates for predictions. However, it may face scalability issues when dealing with large datasets. Despite these challenges, GPR remains valuable in a diverse range of machine learning applications because of its ability to provide insightful predictions and uncertainties.

The machine learning algorithm was prepared in Python programming language using The Scikit-Learn library[152] and run with Jupyter.

All input variables (or features) were defined categorically. The categories used were the same as those detailed in Table 5 for the multiple linear regression models. Dummy (one-hot) coding was used for categorical definition. Twenty percent of the dataset was used to train the algorithm, and 80% was used to validate the algorithm. Additionally, 10-fold cross-validation was employed for all algorithms. This cross-validation technique is crucial for assessing the model's performance by examining how it generalises across different subsets of the data used for training[153,154]

R-square and Mean Square Error values were analysed to evaluate the performance of the model. *R*-square and Mean Square Error and the 10-fold cross-validation values are given in Table 10. In addition, the correlation matrix obtained from KNN regression between inputs and outputs is given in Table 11. In parallel with previous statistical studies, it was observed that the algorithms used could not establish a successful relationship between inputs and outputs.

Discussion

Additively manufactured metals have gained remarkable interest in the industry, and many conventionally

Table 10. Performance assessment of performed AI algorithm.

Machine Learning Algorithm	R square	Mean square Error	10-Fold CVMSE (mean)	10-Fold CVMSE (Std. dev.)
Desicion Tree	−0.11	0.010	0.013	0.003
Gaussiann Process	−0.51	0.015	0.017	0.004
KNN Regression	−0.29	0.013	0.014	0.003
MLP Regression	−0.65	0.016	0.014	0.004
PLS Regression	−0.39	0.014	0.012	0.002
SVM	0.35	0.013	0.015	0.003

manufactured components will be manufactured with additive manufacturing once it reaches the desired specifications. While the literature on the topic is still limited, there are studies exploring the effects of additive manufacturing process parameters on fatigue life. Due to the heterogeneous structure of the parts, the different sub-production methods and their parameters, the effects of these parameters are unclear. Researchers are also focused on enhancing the mechanical properties of additively manufactured components through post-processing methods, especially via heat treatment and surface treatments. Considering the many microvoids created in the structures by additive manufacturing, researchers commonly use hot isostatic pressing (HIP) as a heat treatment method to vanish or lessen the microvoids, which has a positive effect on mechanical strength. However, it should be noted that parameters such as temperature, duration, pressure and environment have restrictions, and their effects can be positive or negative.

This study aimed to establish whether useful design SN curves could be estimated for additively manufactured metals through statistical and machine learning analysis of a large quantity of experimental fatigue data. In this study, a database compiling the papers that studied on fatigue behaviour of additively manufactured metals in the literature[59] was utilised. Stress-fatigue life (*S-N*) curves in the database were re-analysed according to the endurance limit at extrapolated 2.10^6 cycles, and the effects of various parameters on fatigue life were investigated. Due to the high scatter in the graphs, deductions are not straightforward. Consequently, statistical and artificial intelligence analysis methods were employed to identify trends and predict the data.

The mean $\sigma_{\%50}/\sigma_{UTS}$ values for all data sets were 0.18 and 0.21 for R = 0.1 and $R = -1$, respectively, however the scatter was significant. The mean values of the negative inverse slope were obtained as 6.7 and 5.5 for 0.1 and −1 loading ratios, respectively, with 59% of the *k* values falling between 3 and 6. The Gerber, Goodman, Dietman and Eliptical mean stress curves failed to provide a clear correlation of the mean stress data, with some data points falling outside all four curves. Attempts to develop linear

Table 11. Correlation matrix obtained from KNN regression between inputs and outputs.

	k	σ_{UTS}	Direction 0°	Direction 90°	Aluminium	Steel	Titanium	Heat Treated	Non-Heat Treated	Machined	Machined & Polished	As-built	Polished	R = −1	R = 0.1
k	1	0.59	0.04	−0.04	−0.04	0.06	−0.03	−0.03	0.03	0.21	0.03	−0.19	−0.09	−0.08	0.08
σ_{50}/σ_{UTS}	0.59	1	−0.01	0.01	−0.12	0.28	−0.2	0.02	−0.02	0.26	0.05	−0.21	−0.14	0.17	0.17

regression and machine learning models that could predict the endurance limit and negative inverse slope of the fatigue data sets were unsuccessful, with all methods returning R^2 values less than 0.45. As a result, standard design curve rules or predictive models could not be developed for AM metals using the database available. The attempt presented here to train a machine learning model to predict fatigue design curves for AM metals was constrained by the available data and insufficient data was available for important parameters such as the manufacturing processes, material properties, material microstructure and defects. While AI presents a promising solution, our analysis indicates it is necessary to include additional parameters to make reliable fatigue property estimates for AM metals using machine learning. At present experimental fatigue data for the combination of material and manufacturing parameters is still needed for robust fatigue design of AM metal components.

Through the investigations conducted for this study, several quantitative trends were identified in the data, which may benefit from additional investigation. Surface operations consistently appeared to have an effect on the fatigue strengths reported in the data sets, regardless of any other variables, with the effect of a machined surface finish being particularly prominent. Aluminium was the only material to show sensitivity to build direction independently of other parameters, agreeing with the findings of Yadollahi et al.[26] and Zhao et al.[25] Load ratio only appeared as a significant factor in combination with either heat treatment or surface finish for all three metals, which may be explained by the ability of heat treatment and surface operations to remove residual stresses from the as-built material.

Conclusions

To aid designers using 3D-printed metals, this study aimed to establish whether useful design SN curves could be estimated for additively manufactured metals through statistical and machine learning analysis of a large quantity of experimental fatigue data. From the work detailed in this paper the following conclusions were drawn:

- While AI presents a promising solution, our analysis indicates it is likely necessary to account for parameters in addition to those considered here, such as manufacturing processes, material properties, material microstructure and defects to make reliable fatigue property estimates for AM metals using machine learning.
- At present experimental fatigue data for the combination of material and manufacturing parameters is still needed for robust fatigue design of AM metal components.

- Surface operations, particularly surface machining, have a significant effect on the fatigue strength of 3D-printed aluminium, steel and titanium.
- The fatigue strength of 3D-printed aluminium is sensitive to build orientation, whereas steel and titanium are much less sensitive to build orientation.
- Load ratio has a significant effect on the fatigue strength of 3D-printed aluminium, steel and titanium only when coupled with heat treatment (for aluminium and steel) or surface operations (for steel and titanium).
- The mean values of the negative inverse slope were obtained as 6.7 and 5.5 for 0.1 and -1 loading ratios, respectively, with 59% of the k values falling between 3 and 6.

Declaration of conflicting interests

The author(s) declared no potential conflicts of interest with respect to the research, authorship, and/or publication of this article.

Funding

ORCID iDs

Mehmet F Yaren https://orcid.org/0000-0002-7739-0794
Edward John https://orcid.org/0000-0002-8707-4197
Luca Susmel https://orcid.org/0000-0001-7753-9176

References

1. Blakey-Milner B, Gradl P, Snedden G, et al. Metal additive manufacturing in aerospace: a review. *Mater Des* 2021; 209: 110008.
2. Balachandramurthi AR, Moverare J, Dixit N, et al. Influence of defects and as-built surface roughness on fatigue properties of additively manufactured alloy 718. *Mater Sci Eng A* 735: 463–474.
3. Blinn B, Klein M and Beck T. Determination of the anisotropic fatigue behaviour of additively manufactured structures with short-time procedure PhyBaL LIT. *MATEC Web Conf* 2018; 165: 02006.
4. Kumar P, Jayaraj R, Suryawanshi J, et al. Fatigue strength of additively manufactured 316L austenitic stainless steel. *Acta Mater* 2020; 199: 225–239.
5. Masuo H, Tanaka Y, Morokoshi S, et al. Influence of defects, surface roughness and HIP on the fatigue strength of Ti-6Al-4V manufactured by additive manufacturing. *Int J Fatigue* 117: 163–179.
6. Nicoletto G, Konečná R, Frkáň M, et al. Surface roughness and directional fatigue behavior of as-built EBM and DMLS Ti6Al4V. *Int J Fatigue* 116(no): 140–148.
7. Nishikawa H, Furuya Y, Kitano H, et al. In-situ observation of microstructurally small fatigue crack initiation and growth behaviors of additively-manufactured alloy 718. *Mater Sci Eng A* 2022; 835: 142682.
8. Soyama H and Takeo F. Effect of various peening methods on the fatigue properties of titanium alloy Ti6Al4V manufactured by direct metal laser sintering and electron beam melting. *Materials* 2020; 13(10): 1–26. DOI: 10.3390/ma13102216
9. Vayssette B, Saintier N, Brugger C, et al. Surface roughness of Ti-6Al-4V parts obtained by SLM and EBM: Effect on the high cycle fatigue life. *Procedia Eng* 2018; 213: 89–97.
10. Vayssette B, Saintier N, Brugger C, et al. Surface roughness effect of SLM and EBM Ti-6Al-4V on multiaxial high cycle fatigue. *Theor Appl Fract Mech* 108(no): 102581. 2020.
11. Zhao X, Li S, Zhang M, et al. Comparison of the microstructures and mechanical properties of Ti-6Al-4V fabricated by selective laser melting and electron beam melting. *Mater Des* 2016; 95: 21–31.
12. Zhong Y, Rännar LE, Wikman S, et al. Additive manufacturing of ITER first wall panel parts by two approaches: selective laser melting and electron beam melting. *Fusion Eng Des* 2017; 116: 24–33.
13. Blinn B, Lion P, Jordan O, et al. Process-influenced fatigue behavior of AISI 316L manufactured by powder- and wire-based laser direct energy deposition. *Mater Sci Eng A* 2021; 818(no): 141383.
14. Edwards P and Ramulu M. Effect of build direction on the fracture toughness and fatigue crack growth in selective laser melted Ti-6Al-4V. *Fatigue Fract Eng Mater Struct* 2015; 38(10): 1228–1236.
15. Scott-Emuakpor O, Sheridan L, Beck J, et al. Establishing an acceptance criteria for assessing fatigue of additive repair processes. *J Eng Gas Turbine Power* 2021; 143(12): 1–7.
16. Fousová M, Vojtěch D, Doubrava K, et al. Influence of inherent surface and internal defects on mechanical properties of additively manufactured Ti6Al4V alloy: comparison between selective laser melting and electron beam melting. *Materials* 2018; 11(4): 537.
17. Gong H, Rafi K, Gu H, et al. Influence of defects on mechanical properties of Ti–6Al–4V components produced by selective laser melting and electron beam melting. *Mater Des* 2015; 86: 545–554.
18. Greitemeier D, Palm F, Syassen F, et al. Fatigue performance of additive manufactured TiAl6V4 using electron and laser beam melting. *Int J Fatigue* 2017; 94: 211–217.
19. Kahlin M, Ansell H and Moverare JJ. Fatigue behaviour of notched additive manufactured Ti6Al4V with as-built surfaces. *Int J Fatigue* 2017; 101: 51–60.
20. Kahlin M, Ansell H, Basu D, et al. Improved fatigue strength of additively manufactured Ti6Al4V by surface post processing. *Int J Fatigue* 2020; 134: 105497.
21. Stern F, Becker L, Cui C, et al. Improving the defect tolerance of PBF-LB/M processed 316L steel by increasing the nitrogen content. *Adv Eng Mater* 2023; 25(1): 1–13. DOI: 10.1002/adem.202200751
22. Chen C, Araby S, Demiral M, et al. Fatigue behavior and tribological properties of laser additive manufactured aluminum alloy/boron nitride nanosheet nanocomposites. *J Mater Res Technol* 2022; 20: 3930–3948.

23. Zhan Z. Experiments and numerical simulations for the fatigue behavior of a novel TA2-TA15 titanium alloy fabricated by laser melting deposition. *Int J Fatigue* 2018; 121: 20–29.

24. Nezhadfar PD, Thompson S, Saharan A, et al. Structural integrity of additively manufactured aluminum alloys: Effects of build orientation on microstructure, porosity, and fatigue behavior. *Addit Manuf* 2021; 47: 102292.

25. Zhao J, Easton M, Qian M, et al. Effect of building direction on porosity and fatigue life of selective laser melted AlSi12Mg alloy. *Mater Sci Eng A* 2018; 729: 76–85.

26. Yadollahi A, Shamsaei N, Thompson SM, et al. Effects of building orientation and heat treatment on fatigue behavior of selective laser melted 17-4 PH stainless steel. *Int J Fatigue* 2017; 94: 218–235.

27. Persenot T, Burr A, Martin G, et al. Effect of build orientation on the fatigue properties of as-built electron beam melted Ti-6Al-4V alloy. *Int J Fatigue* 2019; 118: 65–76.

28. Sun W, Ma Y, Huang W, et al. Effects of build direction on tensile and fatigue performance of selective laser melting Ti6Al4V titanium alloy. *Int J Fatigue* 2020; 130: 105260.

29. Witkin DB, Patel D, Albright TV, et al. Influence of surface conditions and specimen orientation on high cycle fatigue properties of Inconel 718 prepared by laser powder bed fusion. *Int J Fatigue* 2020; 132: 105392.

30. Qian G, Li Y, Paolino DS, et al. Very-high-cycle fatigue behavior of Ti-6Al-4V manufactured by selective laser melting: Effect of build orientation. *Int J Fatigue* 2020; 136: 105628.

31. Solberg K, Hovig EW, Sørby K, et al. Directional fatigue behaviour of maraging steel grade 300 produced by laser powder bed fusion. *Int J Fatigue* 2021; 149: 106229.

32. Chang K, Liang E, Huang W, et al. Microstructural feature and mechanical property in different building directions of additive manufactured Ti6Al4V alloy. *Mater Lett* 2020; 267: 127516.

33. Bača A, Konečná R, Nicoletto G, et al. Influence of build direction on the fatigue behaviour of Ti6Al4V alloy produced by direct metal laser sintering. *Mater Today Proc* 2016; 3(4): 921–924.

34. Cutolo A, Elangeswaran C, de Formanoir C, et al. Effect of heat treatments on fatigue properties of Ti–6Al–4V and 316L produced by laser powder bed fusion in as-built surface condition. In: *Flavor Physics and the TeV Scale*, 2019, pp.395–405. Cham: Springer.

35. Schneller W, Leitner M, Pomberger S, et al. Fatigue strength assessment of additively manufactured metallic structures considering bulk and surface layer characteristics. *Addit Manuf* 2021; 40: 101930.

36. Kaletsch A, Qin S, Herzog S, et al. Influence of high initial porosity introduced by laser powder bed fusion on the fatigue strength of Inconel 718 after post-processing with hot isostatic pressing. *Addit Manuf* 2021; 47: 102331.

37. Tridello A, Fiocchi Biffi CA, et al. VHCF response of Gaussian SLM AlSi10Mg specimens: Effect of a stress relief heat treatment. *Int J Fatigue* 2019; 124: 435–443.

38. Sprengel M, Bača A, Gumpinger J, et al. Fatigue properties of powder bed fused Inconel 718 in as-built surface condition. In: Correia J, De Jesus A, Fernandes A, et al. (eds) *Mechanical fatigue of metals*. Cham: Springer, 2019, pp.91–97.

39. Ojha A, Lai W-J, Li Z, et al. Defect-based fatigue modeling for AlSi10Mg produced by laser powder bed fusion process. In: *TMS 2021 150th annual meeting & exhibition supplemental proceedings*, 2021, pp.75–91. Cham: Springer.

40. Lai W-J, Ojha A and Li Z. Effect of post heat treatment on fatigue strength of AlSi10Mg produced by laser powder bed fusion process. In: *TMS 2022 151st Annual Meeting & Exhibition Supplemental Proceedings*, 2022, pp.141–163. Cham: Springer.

41. Santos Macías JG, Zhao L, Tingaud D, et al. Hot isostatic pressing of laser powder bed fusion AlSi10Mg: parameter identification and mechanical properties. *J Mater Sci* 2022; 57(21): 9726–9740.

42. Cheng H, Liu D, Tang HB, et al. Effect of hot isostatic pressing on fatigue properties of laser melting deposited AerMet100 steel. *J Iron Steel Res Int* 2013; 20(11): 79–84.

43. Dietrich K, Diller J, Dubiez-Le Goff S, et al. The influence of oxygen on the chemical composition and mechanical properties of Ti-6Al-4V during laser powder bed fusion (L-PBF). *Addit Manuf* 2020; 32: 100980.

44. Ardi DT, Guowei L, Maharjan N, et al. Effects of post-processing route on fatigue performance of laser powder bed fusion Inconel 718. *Addit Manuf* 2020; 36: 101442.

45. Schneller W, Leitner M, Leuders S, et al. Fatigue strength estimation methodology of additively manufactured metallic bulk material. *Addit Manuf* 2021; 39: 101688.

46. Rautio T, Jaskari M, Gundgire T, et al. The effect of severe shot peening on fatigue life of laser powder bed fusion manufactured 316L stainless steel. *Materials* 2022; 15(10): 3517.

47. Nezhadfar PD, Shrestha R, Phan N, et al. Fatigue behavior of additively manufactured 17-4 PH stainless steel: synergistic effects of surface roughness and heat treatment. *Int J Fatigue* 2019; 124: 188–204.

48. Croccolo D, De Agostinis M, Fini S, et al. Effects of machining and heat and surface treatments on as built DMLS processed maraging steel. In: *Proceedings of the first international conference on theoretical, applied and experimental mechanics*, 2019, pp.110–111.

49. Nakamura M, Takahashi K and Saito Y. Effect of shot and laser peening on fatigue strength of additively manufactured aluminum alloy with rough surfaces. *J Mater Eng Perform* 2023; 32(4): 1589–1600.

50. Tezel T. Fatigue life improvement of 3D-printed aluminum by electroplating with nickel. *JOM* 2022; 74(3): 748–754.

51. Concli F, Fraccaroli L, Nalli F, et al. High and low-cycle-fatigue properties of 17–4 PH manufactured via selective laser melting in as-built, machined and hipped conditions. *Prog Addit Manuf* 2022; 7(1): 99–109.

52. Ghiotti A, Bertolini R, Sorgato M, et al. Ti6Al4V titanium alloy fatigue strength after AM- and machining-based process chains. *CIRP Ann* 2022; 71(1): 461–464.

53. Childerhouse T, Hernández-Nava E, Tapoglou N, et al. The influence of finish machining depth and hot iso-static pressing on defect distribution and fatigue behaviour of selective electron beam melted Ti-6Al-4V. *Int J Fatigue* 2021; 147: 106169.

54. Yu C, Huang Z, Zhang Z, et al. Effects of sandblasting and HIP on very high cycle fatigue performance of SLM-fabricated IN718 superalloy. *J Mater Res Technol* 2022; 18: 29–43.

55. Baek M-S, Kreethi R, Park T-H, et al. Influence of heat treatment on the high-cycle fatigue properties and fatigue damage mechanism of selective laser melted AlSi10Mg alloy. *Mater Sci Eng A* 2021; 819: 141486.

56. Mishurova T, Artzt K, Rehmer B, et al. Separation of the impact of residual stress and microstructure on the fatigue performance of LPBF Ti-6Al-4V at elevated temperature. *Int J Fatigue* 2021; 148: 106239.

57. Lee S, Ahmadi Z, Pegues JW, et al. Laser polishing for improving fatigue performance of additive manufactured Ti-6Al-4V parts. *Opt Laser Technol* 2021; 134: 106639.

58. Balbaa M, Ghasemi A, Fereiduni E, et al. Improvement of fatigue performance of laser powder bed fusion fabricated IN625 and IN718 superalloys via shot peening. *J Mater Process Technol* 2022; 304: 117571.

59. Zhang Z and Xu Z. Fatigue database of additively manufactured alloys. *Sci Data* 2023; 10(1): 249.

60. Kedziora S, Decker T, Museyibov E, et al. Strength properties of 316L and 17-4 PH stainless steel produced with additive manufacturing. *Materials* 2022; 15(18): 6278.

61. Barr C, Rashid RAR, Da Sun S, et al. Role of deposition strategy and fill depth on the tensile and fatigue performance of 300 M repaired through laser directed energy deposition. *Int J Fatigue* 2021; 146: 106135.

62. Zhang M, Sun C-N, Zhang X, et al. High cycle fatigue and ratcheting interaction of laser powder bed fusion stainless steel 316L: fracture behaviour and stress-based modelling. *Int J Fatigue* 2019; 121: 252–264.

63. Zhang M, Sun CN, Zhang X, et al. High cycle fatigue life prediction of laser additive manufactured stainless steel: a machine learning approach. *Int J Fatigue* 2019; 128: 105194.

64. Afkhami S, Dabiri M, Piili H, et al. Effects of manufacturing parameters and mechanical post-processing on stainless steel 316L processed by laser powder bed fusion. *Mater Sci Eng A* 2021; 802: 140660.

65. Spierings AB, Starr TL and Wegener K. Fatigue performance of additive manufactured metallic parts. *Rapid Prototyp J* 2013; 19(2): 88–94.

66. Solberg K, Guan S, Razavi N, et al. Fatigue of additively manufactured 316L stainless steel: the influence of porosity and surface roughness. *Fatigue Fract Eng Mater Struct* 2019; 42(9): 2043–2052.

67. Thawon I, Fongsamootr T, Mona Y, et al. Investigation of the mechanical properties of additively manufactured metal parts with different relative densities. *Appl Sci* 2022; 12(19): 9915.

68. Voloskov B, Evlashin S, Dagesyan S, et al. Very high cycle fatigue behavior of additively manufactured 316L stainless steel. *Materials* 2020; 13(15): 3293.

69. He P, Webster RF, Yakubov V, et al. Fatigue and dynamic aging behavior of a high strength Al-5024

70. Lasagni F, Galleguillos C, Herrera M, et al. On the processability and mechanical behavior of Al–Mg–Sc alloy for PBF-LB. *Prog Addit Manuf* 2022; 7(1): 29–39.

71. Qin Z, Kang N, El Mansori M, et al. Anisotropic high cycle fatigue property of Sc and Zr-modified Al-Mg alloy fabricated by laser powder bed fusion. *Addit Manuf* 2022; 49: 102514.

72. Qin Z, Kang N, Zong H, et al. Improved fatigue properties of laser powder bed fusion of Al–4.74Mg–0.70Sc–0.32Zr alloy via hot isostatic pressing. *Mater Res Lett* 2022; 10(11): 720–727.

73. Wu Z, Wu S, Bao J, et al. The effect of defect population on the anisotropic fatigue resistance of AlSi10Mg alloy fabricated by laser powder bed fusion. *Int J Fatigue* 2021; 151: 106317.

74. Qian W, Wu S, Wu Z, et al. In situ X-ray imaging of fatigue crack growth from multiple defects in additively manufactured AlSi10Mg alloy. *Int J Fatigue* 2022; 155: 106616.

75. Peng X, Wu S, Qian W, et al. The potency of defects on fatigue of additively manufactured metals. *Int J Mech Sci* 2022; 221: 107185.

76. Yan Q, Song B and Shi Y. Comparative study of performance comparison of AlSi10Mg alloy prepared by selective laser melting and casting. *J Mater Sci Technol* 2020; 41: 199–208.

77. Beretta S, Patriarca L, Gargourimotlagh M, et al. A benchmark activity on the fatigue life assessment of AlSi10Mg components manufactured by L-PBF. *Mater Des* 2022; 218: 110713.

78. Zhang Y, Feng E, Mo W, et al. On the microstructures and fatigue behaviors of 316L stainless steel metal injection molded with gas- and water-atomized powders. *Metals* 2018; 8(11): 893.

79. Rao JH, Zhang Y, Huang A, et al. Improving fatigue performances of selective laser melted Al-7Si-0.6Mg alloy via defects control. *Int J Fatigue* 2019; 129: 105215.

80. Cacace S, Gökhan Demir A, Sala G, et al. Influence of production batch related parameters on static and fatigue resistance of LPBF produced alsi7mg0.6. *Int J Fatigue* 2022; 165: 107227.

81. Wang J, Zhang M, Wang B, et al. Influence of surface porosity on fatigue life of additively manufactured ASTM A131 EH36 steel. *Int J Fatigue* 2021; 142: 105894.

82. Wang J, Zhang M, Tan X, et al. Fatigue behavior of ASTM A131 EH36 steel samples additively manufactured with selective laser melting. *Mater Sci Eng A* 2020; 777: 139049.

83. Okazaki Y. Effects of fine microstructures and precipitates of laser-sintered Co–28Cr–6Mo alloy femoral components on wear rate of UHMWPE inserts in a knee joint simulator. *J Mech Behav Biomed Mater* 2020; 112: 103998.

84. Wai Cho HH, Takaichi A, Kajima Y, et al. Effect of post-heat treatment cooling conditions on microstructures and fatigue properties of cobalt chromium molybdenum alloy fabricated through selective laser melting. *Metals* 2021; 11(7): 1005.

85. Kuzminova YO, Firsov DG, Dagesyan SA, et al. Fatigue behavior of additive manufactured CrFeCoNi

medium-entropy alloy. *J Alloys Comp* 2021; 863: 158609.

86. He C, Wei J, Li Y, et al. Improvement of microstructure and fatigue performance of wire-arc additive manufactured 4043 aluminum alloy assisted by interlayer friction stir processing. *J Mater Sci Technol* 2023; 133: 183–194.

87. Xie C, Wu S, Yu Y, et al. Defect-correlated fatigue resistance of additively manufactured Al-Mg4.5Mn alloy with in situ micro-rolling. *J Mater Process Technol* 2021; 291: 117039.

88. Shao WW, Zhang B, Liu Y, et al. Effect of laser power on porosity and mechanical properties of GH4169 fabricated by laser melting deposition. *Tungsten* 2019; 1(4): 297–305.

89. Han Q, Mertens R, Montero-Sistiaga ML, et al. Laser powder bed fusion of Hastelloy X: Effects of hot isostatic pressing and the hot cracking mechanism. *Mater Sci Eng A* 2018; 732: 228–239.

90. Poulin J-R, Kreitcberg A, Terriault P, et al. Fatigue strength prediction of laser powder bed fusion processed Inconel 625 specimens with intentionally-seeded porosity: Feasibility study. *Int J Fatigue* 2020; 132: 105394.

91. Theriault A, Xue L and Dryden JR. Fatigue behavior of laser consolidated IN-625 at room and elevated temperatures. *Mater Sci Eng A* 2009; 516: 217–222.

92. Klein Fiorentin F, Maciel D, Gil J, et al. Fatigue assessment of Inconel 625 produced by directed energy deposition from miniaturized specimens. *Metals* 2022; 12(1): 156.

93. Sarkar R, Chen B, Fitzpatrick ME, et al. Additive manufacturing-based repair of IN718 superalloy and high-cycle fatigue assessment of the joint. *Addit Manuf* 2022; 60: 103276.

94. Wan HY, Yang WK, Wang LY, et al. Toward qualification of additively manufactured metal parts: tensile and fatigue properties of selective laser melted inconel 718 evaluated using miniature specimens. *J Mater Sci Technol* 2022; 97: 239–253.

95. Sabelkin VP, Cobb GR, Shelton TE, et al. Mitigation of anisotropic fatigue in nickel alloy 718 manufactured via selective laser melting. *Mater Des* 2019; 182: 108095.

96. Musekamp J, Reiber T, Hoche HC, et al. Influence of LPBF surface characteristics on fatigue properties of scalmalloy. *Metals* 2021; 11(12): 1961.

97. Shin C-S, Do T, Lee D, et al. A comparative study on mechanical properties of fully dense 420 stainless steel parts produced by modified binder jet printing. *Mater Des* 2022; 224: 111343.

98. Zhou L, Yuan T, Li R, et al. Densification, microstructure evolution and fatigue behavior of Ti-13Nb-13Zr alloy processed by selective laser melting. *Powder Technol* 2019; 342: 11–23.

99. Benedetti M, Fontanari V, Bandini M, et al. Low- and high-cycle fatigue resistance of Ti-6Al-4V ELI additively manufactured via selective laser melting: mean stress and defect sensitivity. *Int J Fatigue* 2018; 107: 96–109.

100. Biswal R, Zhang X, Syed AK, et al. Criticality of porosity defects on the fatigue performance of wire + arc additive manufactured titanium alloy. *Int J Fatigue* 2019; 122: 208–217.

101. Le V-D, Pessard E, Morel F, et al. Fatigue behaviour of additively manufactured Ti-6Al-4V alloy: the role of defects on scatter and statistical size effect. *Int J Fatigue* 2020; 140: 105811.

102. Syed AK, Zhang X, Caballero A, et al. Influence of deposition strategies on tensile and fatigue properties in a wire + arc additive manufactured Ti-6Al-4V. *Int J Fatigue* 2021; 149: 106268.

103. Franchitti S, Pirozzi C and Borrelli R. Influence of hot isostatic pressing and surface finish on the mechanical behaviour of Ti6Al4V processed by electron beam melting. *Fatigue Fract Eng Mater Struct* 2020; 43(12): 2828–2841.

104. Brika SE and Brailovski V. Influence of powder particle morphology on the static and fatigue properties of laser powder bed-fused Ti-6Al-4V components. *J Manuf Mater Process* 2020; 4(4): 107.

105. Wanjara P, Backman D, Sikan F, et al. Microstructure and mechanical properties of Ti-6Al-4V additively manufactured by electron beam melting with 3D part nesting and powder reuse influences. *J Manuf Mater Process* 2022; 6(1): 21.

106. Jimenez EH, Kreitcberg A, Moquin E, et al. Influence of post-processing conditions on the microstructure, static, and fatigue resistance of laser powder bed fused Ti-6Al-4V components. *J Manuf Mater Process* 2022; 6(4): 85.

107. Segurajauregi U, Álvarez-Vázquez A, Muñiz-Calvente M, et al. Fatigue assessment of selective laser melted Ti-6Al-4V: influence of speed manufacturing and porosity. *Metals* 2021; 11(7): 1022.

108. Springer S, Leitner M, Gruber T, et al. Fatigue assessment of wire and arc additively manufactured Ti-6Al-4V. *Metals* 2022; 12(5): 795.

109. Nezhadfar PD, Anderson-Wedge K, Daniewicz SR, et al. Improved high cycle fatigue performance of additively manufactured 17-4 PH stainless steel via in-process refining micro-/defect-structure. *Addit Manuf* 2020; 36: 101604.

110. Carneiro L, Jalalahmadi B, Ashtekar A, et al. Cyclic deformation and fatigue behavior of additively manufactured 17–4 PH stainless steel. *Int J Fatigue* 2019; 123: 22–30.

111. Molaei R, Fatemi A and Phan N. Multiaxial fatigue of LB-PBF additive manufactured 17–4 PH stainless steel including the effects of surface roughness and HIP treatment and comparisons with the wrought alloy. *Int J Fatigue* 2020; 137: 105646.

112. Yadollahi A, Mahmoudi M, Elwany A, et al. Fatigue-life prediction of additively manufactured material: Effects of heat treatment and build orientation. *Fatigue Fract Eng Mater Struct* 2020; 43(4): 831–844.

113. Damon J, Hanemann T, Dietrich S, et al. Orientation dependent fatigue performance and mechanisms of selective laser melted maraging steel x3nicomoti18-9-5. *Int J Fatigue* 2019; 127: 395–402.

114. Elangeswaran C, Gurung K, Koch R, et al. Post-treatment selection for tailored fatigue performance of 18Ni300 maraging steel manufactured by laser powder bed fusion. *Fatigue Fract Eng Mater Struct* 2020; 43(10): 2359–2375.

115. Lai W-J, Ojha A, Li Z, et al. Effect of residual stress on fatigue strength of 316L stainless steel produced by

laser powder bed fusion process. *Prog Addit Manuf* 2021; 6(3): 375–383.

116. Elangeswaran C, Cutolo A, Gallas S, et al. Predicting fatigue life of metal LPBF components by combining a large fatigue database for different sample conditions with novel simulation strategies. *Addit Manuf* 2022; 50: 102570.

117. Elangeswaran C, Cutolo A, Muralidharan GK, et al. Effect of post-treatments on the fatigue behaviour of 316L stainless steel manufactured by laser powder bed fusion. *Int J Fatigue* 2019; 123: 31–39.

118. Blinn B, Ley M, Buschhorn N, et al. Investigation of the anisotropic fatigue behavior of additively manufactured structures made of AISI 316L with short-time procedures PhyBaLLIT and phybalcht. *Int J Fatigue* 2019; 124: 389–399.

119. Blinn B, Krebs F, Ley M, et al. Determination of the influence of a stress-relief heat treatment and additively manufactured surface on the fatigue behavior of selectively laser melted AISI 316L by using efficient short-time procedures. *Int J Fatigue* 2020; 131: 105301.

120. Kotzem D, Kleszczynski S, Stern F, et al. Impact of single structural voids on fatigue properties of AISI 316L manufactured by laser powder bed fusion. *Int J Fatigue* 2021; 148: 106207.

121. Yu C, Zhang P, Zhang Z, et al. Microstructure and fatigue behavior of laser-powder bed fusion austenitic stainless steel. *J Mater Sci Technol* 2020; 46: 191–200.

122. Uematsu Y, Sasaki R, Kakiuchi T, et al. Fatigue design curves for laser-metal-deposited type 420 stainless steel and effect of an interval during deposition process. *Int J Adv Manuf Technol* 2021; 116(9–10): 2917–2927.

123. Romano S, Brückner-Foit A, Brandão A, et al. Fatigue properties of AlSi10Mg obtained by additive manufacturing: defect-based modelling and prediction of fatigue strength. *Eng Fract Mech* 2018; 187: 165–189.

124. Zhang C, Zhu H, Liao H, et al. Effect of heat treatments on fatigue property of selective laser melting AlSi10Mg. *Int J Fatigue* 2018; 116: 513–522.

125. Domfang Ngnekou JN, Nadot Y, Henaff G, et al. Fatigue properties of AlSi10Mg produced by Additive Layer Manufacturing. *Int J Fatigue* 2019; 119: 160–172.

126. Muhammad M, Nezhadfar PD, Thompson S, et al. A comparative investigation on the microstructure and mechanical properties of additively manufactured aluminum alloys. *Int J Fatigue* 2021; 146: 106165.

127. Sausto F, Carrion PE, Shamsaei N, et al. Fatigue failure mechanisms for AlSi10Mg manufactured by L-PBF under axial and torsional loads: the role of defects and residual stresses. *Int J Fatigue* 2022; 162: 106903.

128. Awd M, Stern F, Kampmann A, et al. Microstructural characterization of the anisotropy and cyclic deformation behavior of selective laser melted AlSi10Mg structures. *Metals* 2018; 8(10): 825.

129. Yamashita Y, Murakami T, Mihara R, et al. Defect analysis and fatigue design basis for Ni-based superalloy 718 manufactured by selective laser melting. *Int J Fatigue* 2018; 117: 485–495.

130. Liu SY, Shao S, Guo H, et al. The microstructure and fatigue performance of Inconel 718 produced by laser-based powder bed fusion and post heat treatment. *Int J Fatigue* 2022; 156: 106700.

131. Yu X, Lin X, Wang Z, et al. Room and high temperature high-cycle fatigue properties of Inconel 718 superalloy prepared using laser directed energy deposition. *Mater Sci Eng A* 2021; 825: 141865.

132. Doh J, Raju N, Raghavan N, et al. Bayesian inference-based decision of fatigue life model for metal additive manufacturing considering effects of build orientation and post-processing. *Int J Fatigue* 2022; 155: 106535.

133. Meneghetti G, Rigon D, Cozzi D, et al. Influence of build orientation on static and axial fatigue properties of maraging steel specimens produced by additive manufacturing. *Procedia Struct Integr* 2017; 7: 149–157.

134. Wei K, Wang Z and Zeng X. Preliminary investigation on selective laser melting of Ti-5Al-2.5Sn α-Ti alloy: from single tracks to bulk 3D components. *J Mater Process Technol* 2017; 244: 73–85.

135. Kaya MŞ, Ece RE, Keles O, et al. Effect of post processes on mechanical properties of 3D printed Ti6Al4V gears. *J Mater Eng Perform* 2022; 31(8): 6300–6309.

136. Bhandari L and Gaur V. On study of process induced defects-based fatigue performance of additively manufactured Ti6Al4V alloy. *Addit Manuf* 2022; 60: 103227.

137. Karimi J, Antonov M, Kollo L, et al. Role of laser remelting and heat treatment in mechanical and tribological properties of selective laser melted Ti6Al4V alloy. *J Alloys Comp* 2022; 897: 163207.

138. Singla AK, Banerjee M, Sharma A, et al. Selective laser melting of Ti6Al4V alloy: process parameters, defects and post-treatments. *J Manuf Process* 2021; 64: 161–187.

139. Williams MB, Robinson TW, Williamson CJ, et al. Elucidating the effect of additive friction stir deposition on the resulting microstructure and mechanical properties of magnesium alloy we43. *Metals* 2021; 11(11): 1739.

140. Sinclair GM and Dolan TJ. Effect of stress amplitude on statistical variability in fatigue life of 75S-T6 aluminum alloy. *J Fluid Eng* 1953; 75(5): 867–870.

141. Natrella MG. *Experimental statistics*. Washington: Dover Publications Inc, 2005.

142. Anonymous. *Minitab: data analysis, statistical & process improvement tools, version 17*. State College, PA: Minitab Inc.

143. Draper NR and Smith H (eds). *Applied regression analysis*. 3rd ed. Toronto, Canada: John Wiley Sons, 1998.

144. Montgomery DC, P EA and Vining GG (eds). *Introduction to linear regression analysis*. 5th ed. Hoboken, NJ: John & Wiley Sons, 2012.

145. Rokach L and Maimon O. *Data mining with decision trees*. Singapore: World Scientific, 2014, vol. 81.

146. Campbell C and Ying Y. *Learning with support vector machines*. San Rafael, CA: Morgan & Claypool Publishers, 2011.

147. Altman NS. An introduction to kernel and nearest-neighbor nonparametric regression. *Am Stat* 1992; 46(3): 175–185.

148. Marsland S. *Machine learning*. Boca Raton, FL: Chapman and Hall/CRC, 2011.
149. Wegelin JA. "A survey of Partial Least Squares (PLS) methods, with emphasis on the two-block case," 2000.
150. Albak B, Erden C, Ünal O, et al. Welding strength prediction in nuts to sheets joints: machine learning and ANFIS comparative analysis. *Int J Interact Des Manuf* 2024: 1–16. DOI: 10.1007/s12008-024-01805-2
151. Rasmussen CE and Christopher KW. *Gaussian processes for machine learning*. Cambridge, MA: MIT Press, 2006.
152. Pedregosa F, et al. Scikit-Learn: machine learning in Python. *J Mach Learn Res* 2011; 12(10): 2825–2830.
153. Shah M, Borade H, Dave V, et al. Utilizing TGAN and ConSinGAN for improved tool wear prediction: a comparative study with ED-LSTM, GRU, and CNN models. *Electronics* 2024; 13(17): 3484.
154. Falessi D, Huang J, Narayana L, et al. On the need of preserving order of data when validating within-project defect classifiers. *Empir Softw Eng* 2020; 25(6): 4805–4830.